analytical chemistry

Review

pubs.acs.org/ac

Molecular Approaches to Chromatography Using Single Molecule Spectroscopy

Lydia Kisley[†] and Christy F. Landes*[,†,‡]

[†]Department of Chemistry and [‡]Department of Electrical and Computer Engineering, Rice Quantum Institute, Rice University, 6100 Main Street, MS-60, Houston, Texas 77005, United States

CONTENTS

Chromatography is an important analytical technique for the separation of molecules in environmental, pharmaceutical, medicinal, natural product synthesis research, and industrial production. Despite chromatography's extensive use, the selection of appropriate column conditions is driven by empirical methods and phenomenological theories. Single molecule spectroscopy (SMS) offers the possibility to extract molecular-scale data, with the overall goals of obtaining a mechanistic understanding of chromatography and providing a framework for intelligent chromatographic optimization, neither of which is achievable through traditional ensemble-averaged methods. Here we review both the spectroscopic techniques and the new insights that SMS has provided on interfacial liquid chromatographic separations. The experimental studies include reverse phase, normal phase (silica based), and ion-exchange chromatography. We discuss how single molecule results can inform theory and predict column performance and a perspective of future directions in the field is given. Overall, this review demonstrates the value of collaborations between the separations and single molecule spectroscopy communities and hopefully will inspire future efforts to achieve a molecular-scale understanding of the crucial analytical technique of chromatography.

Chromatographic separation of molecules from complex mixtures is an important analytical technique. In the pharmaceutical industry, chromatography is used to isolate therapeutic biomolecules produced by recombinant-engineered bacteria for safe products to be consumed by patients.[1] Similarly, in the natural food product industry, chromatography can quantify the amount of antioxidants or beneficial lipid products in fortified food used for maintaining health.[2] Chromatographic methods are crucial in these two industries that combined accounted for over $120 billion dollars to the economy in 2009.[3,4] Chromatography also has important roles in the oil and gas industry,[5] environmental analysis,[6] and natural product synthesis. Thus, as one of the most commonly used analysis techniques spanning many applications,[7] understanding and improving chromatography has important scientific and economic implications.

Recent advancements in chromatography address the needs of these diverse applications. Liquid chromatography column stationary phases improved by decreasing the particle size to <2 μm,[8] using solid core-porous shell particle geometries,[9] utilizing slip-flow properties of the mobile phase along the stationary phase column walls,[10−12] combining hydrophilic bonded phases and ionic ligands for mixed-mode capabilities,[13] and using monolithic materials[14] to decrease data acquisition times, pressure requirements, and column lengths.[7,15] In improving data analysis, multidimensional methods improved quantification of analytes from nonuniform peaks due to background contributions, retention time shifts, and peak shape changes.[16] Theoretically, numerical and molecular mechanical modeling of analyte adsorption are used to understand plate- and mass-transfer descriptions of column performance.[17,18]

Despite the importance of and advancements in chromatography, an experimental molecular-scale understanding is lacking. In industry, selection of appropriate mobile and stationary phase conditions is often empirically determined through a time-intensive, costly process of testing numerous combinations of variables such as stationary phase packing density, ligand loading, and particle size; mobile phase ionic strength, hydrophobicity, and pH; and column length, diameter, and flow rate. Current explanations of chromatographic performance through theoretical models have relied heavily on phenomenological descriptions that use either variables that have no clear physical parallel within the experiment or broad definitions of diffusion, packing, and

Special Issue: Fundamental and Applied Reviews in Analytical Chemistry 2015

Published: November 14, 2014

   dx.doi.org/10.1021/ac5039225 | *Anal. Chem.* 2015, 87, 83−98

kinetics comprised of many complicated molecular processes contributing in sum. One cause of the lack of mechanistic information in both chromatographic experiment and theory is ensemble averaging. The ensemble averaged information obtained from classical analysis of a vast number of molecules inherently averages out any underlying analyte and/or process heterogeneity.[19] Ensemble methods therefore make it difficult to resolve a fundamental, molecular viewpoint of the potentially heterogeneous processes that occur in practical chromatographic separations.

SMS is a technique that can fill this gap. By observing one molecule at a time, heterogeneity that is hidden in ensemble-averaged studies can be revealed. For example, non-Gaussian peaks due to fronting or tailing are a challenge in chromatography (Figure 1, solid line) and arise from multiple sub-

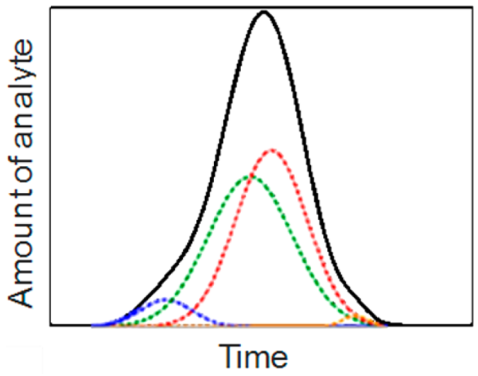

Figure 1. Illustration of asymmetric chromatography peak that at the ensemble level (solid line) cannot resolve the heterogeneous, multiple populations present (dashed lines) that SMS can reveal.

populations of dynamic interactions between the analyte and stationary phase. SMS can resolve individual events that correlate and distinguish the subpopulations (Figure 1, dashed lines), revealing the causes of peak broadening and asymmetry in chromatography from a mechanistic perspective not possible through traditional techniques. Therefore, SMS represents a promising path to a genuinely predictive, molecular understanding of the chromatography processes.

We will review the recent work in relevant SMS techniques with applications to chromatography. Work from the first reports on SMS chromatography in 1998 to the present are included but recent advancements from 2014 that use super-resolution imaging, particle tracking, and relating experimental results to theory will be highlighted. First, the underlying principles of the applicable SMS instrumentation will be summarized. Next, we will highlight specific examples of the application of SMS in providing mechanistic insight into separation methods. Throughout, we will discuss techniques and problems that have been addressed and identify scientific questions that still remain for future collaborations between the separations and SMS fields.

PRINCIPLES OF SINGLE MOLECULE SPECTROSCOPY AND INSTRUMENTAL TECHNIQUES

SMS allows for the detection of an individual molecule, the fundamental concentration detection limit, allowing access to molecular parameters and statistical distributions not available to the ensemble. SMS was first introduced with the foundational work from Moerner[20] and Orrit[21] detecting single molecules at cryogenic temperatures. During the quarter of a century since the technique was first demonstrated, capabilities at room temperature,[22−27] in biological systems,[28,29] and improved temporal[30,31] and spatial[32,33] resolutions have been developed. This section serves as a general introduction to the SMS techniques that have been applied to interfacial studies of liquid chromatography. More detailed reviews of the spectroscopic instrumentation and analysis are available by Moerner and Fromm[19] and Orrit et al.,[34] to name a few. Reviews regarding the specific instrumentation and analysis discussed in this section are also provided.

General Considerations and Sample Requirements. Appropriate sample conditions in fluorescent microscopy allows for single molecule detection. Compared to alternative spectroscopic phenomena such as adsorption, Raman, or Rayleigh scattering, fluorescence with appropriate high quantum yield fluorophores can achieve high signals ($\sim 10^5$ photons/s). The emitted photons are red-shifted from the laser excitation, allowing the emission to be separated from the excitation for detection. A low probe concentration, usually in the picomolar to nanomolar range, is required to ensure only one molecule is detected at a time. The sample must also be as free as possible from contamination and defects, as Raman scattering and fluorescence from impurities decrease the signal-to-background ratio. The chemistry of the fluorescent probe must be appropriate to the system of interest. For example, for the separation of small, charged, organic molecules, the fluorophores themselves can serve as appropriate model molecules. Rhodamine 6G, BODIPY, or Alexa dyes can act as cationic, neutral, or anionic model analytes, respectively.[35] Alternatively, for the separation of biomolecules, natural or modified fluorescent proteins, such as green fluorescent protein,[36,37] are used. For each method, it is important to reduce as much as possible the perturbations to both probe and biomolecular function that are associated with labeling. Proteins can be labeled on native amino acids or mutated to contain a site-specific amino acid. Typically, lysine or cysteine residues are labeled through amine- or thiol-specific chemistry, respectively.[38] Because of the popularity of the SMS and prevalence of fluorescence in biology, a large library of labeling probes is available through companies such as Invitrogen. For further discussion of labeling biological molecules, see Weiss.[39]

Creative solutions to improve or exploit the photophysical drawbacks of fluorescence imaging have been presented in both sample and instrument forms. Single molecule fluorescence is inherently limited by photoblinking and photobleaching when a fluorophore enters a temporary or permanent dark state, respectively, either of which renders the probe useless for observation. Photophysics can limit the amount of data collected or lead to false analysis results; therefore, it is desirable to increase the single molecule fluorescent lifetime. Solution-based approaches have prevented photodynamic reactions where a combination of light and oxygen interact with the fluorophore and cause oxidative damage. Chemical methods have removed oxygen that either reacts as a free radical with the fluorophore or quenches excited fluorophores from solution, commonly using enzymatic-based scavenging solutions.[40] A myriad of different solution cocktails[41−46] and protective strategies[47,48] have been offered and compared.[49] When using chemical approaches, it is important to consider how the requisite pH and/or ionic conditions of the oxygen scavenging solution are compatible with the sample. Alternatively, hardware approaches can be used to reduce adverse photophysics. The excitation intensity can simply

dx.doi.org/10.1021/ac5039225 | Anal. Chem. 2015, 87, 83−98

be decreased, as the number of emitted photons per second increases linearly with incident intensity before reaching a saturating value.[50,51] Reduced excitation intensity will indeed extend the observation time but with the sacrifice of decreasing the signal-to-noise ratio. Therefore, excitation power should be selected to balance between reducing photophysical effects and obtaining adequate signal-to-noise ratio. Other hardware-based approaches that prevent unnecessary excitation of single moleucle fluorophores have been presented through modulating the excitation in sync with the time-gated data acquisition and inherent data conversion time of the detector.[52,53] The signal-to-background ratio can also be improved by modulation of the dark and light state populations of a fluorophore using a modulated secondary laser to resolve signal from the autofluorescent background.[54−56] Finally, synthetic development of new fluorophores, both organic[57−59] and biological,[60] offers improved lifetimes as another route toward better fluorophores.

Confocal Microscopy. In the study of chromatography at the single molecule level, two different fluorescence microscopy geometries have been applied (Figure 2): confocal microscopy and wide field total internal reflection fluorescence (TIRF). In confocal microscopy, the excitation overfills the back of a high numerical aperture objective, leading to the focal volume being focused to the diffraction limit (Figure 2A) with a beam radius of ~200 nm and femtoliter volume. The focal volume can be held stationary and molecules detected as they diffuse through or the objective/sample stage can be scanned to obtain spatial information. Emitted photons are detected on a single-element detector, usually a semiconductor-based avalanche photodiode (APD), though photomultiplier tubes have also been used historically.[61] The resulting signal can be the number of photons detected over time (Figure 2B) or single photons and their arrival time detected in a time-correlated single-photon counting (TCSPC) setup.[62]

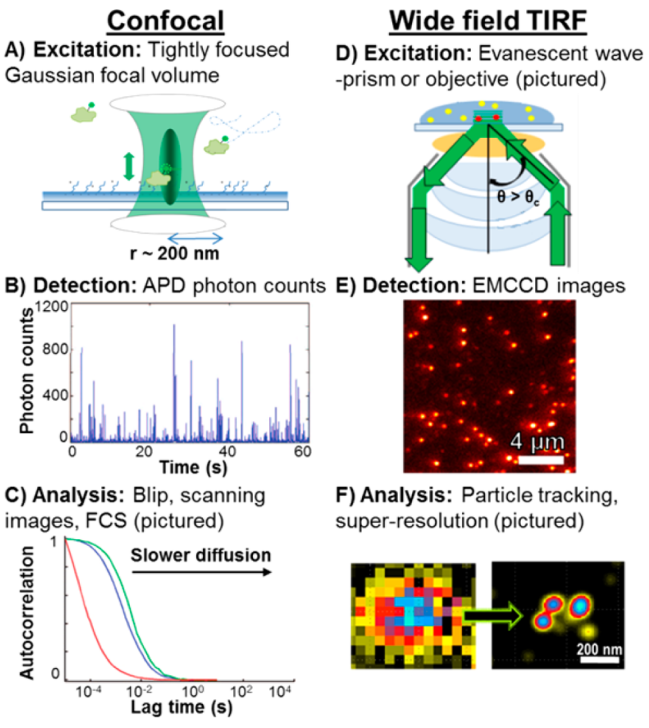

Figure 2. Summary of SMS instrumentation, data, and analysis. (A−C) Representation of confocal microscopy. (A) Excitation geometry at an ion-exchange interface where fluorescently-labeled proteins are being detected. (B) Example intensity trace from 1D detection of photons with an APD detector. (C) Example of FCS analysis where slower diffusion is observed by increasing the probe size (red < blue < green). (D−F) Representation of wide field TIRF microscopy. (D) Through-the-objective TIRF excitation geometry where excitation at a high angle (θ) creates an evanescent wave that only excites fluorophores (red) near the interface, while out of focus fluorophores (yellow) do not contribute to background signal. (E) Example 2D image of single molecules detected on an EMCCD. (F) Analysis of data by super-resolution imaging, improving the spatial resolution from ~250 nm to ~30 nm.

The intensity transient signal (Figure 2B) detected in confocal microscopy reveals single molecule dynamics through several routes of analysis. In the scanning geometry, discussed above, the resulting output from the single channel detector can be reconstructed into an image based on the location of the objective on the sample at a given time. The areas of the image with bright spots reveal the spatial locations of adsorbed molecules. The frequency at which an image can be obtained is limited by the scan rate. Typical acquisition rates can be ~30 mHz for a 15 μm × 15 μm image. Alternatively, when the focal volume is in a fixed location, blip analysis can reveal the frequency of events. Blip analysis simply counts the number of events where increases in intensity, or "blips", indicate that a molecule has passed through the focal volume. The total number of blips can reveal information about the affinity and intermolecular forces at work between the probe molecule and the interface.

Fluorescence correlation spectroscopy (FCS) analysis quantifies diffusion properties of molecules using confocal microscopy. Through not truly a single molecule technique, the correlation of the signal of many single molecule events over time can be related to the time scale of motion of the probes. The results provide a bridge between the classical ensemble averaged and single molecule levels.[63] From the transient signal, $F(t)$, the fluctuations of the signal, $\delta F(t)$ are calculated by subtracting the average signal, $\langle F \rangle$, from all points:

$$\delta F(t) = F(t) - \langle F \rangle \tag{1}$$

The self-similarity of the signal is then calculated through autocorrelation analysis:

$$G(\tau) = \frac{\langle \delta F(t) \delta F(t+\tau) \rangle}{\langle F(t) \rangle^2} \tag{2}$$

where the resulting response, $G(\tau)$, is a result of the overlay of the original signal, $\delta F(t)$, with its shifted self, $\delta F(t+\tau)$, for a given lag time, τ. The resulting autocorrelation decay curve calculated in eq 2 can then be related to the diffusion dynamics of the molecules by fitting to

$$G(\tau) = 1/V_{\text{eff}}\langle C \rangle \left(1 + \frac{\tau}{\tau_D}\right)\left(1 + \left(\frac{r_0}{z_0}\right)^2 \left(\frac{\tau}{\tau_D}\right)\right)^{1/2} \tag{3}$$

where V_{eff} is the size of the effective focal volume, $\langle C \rangle$ is the concentration of fluorescent probe used, τ is the correlation lag time, τ_D is the characteristic diffusion time, and r_0 and z_0 are the focal beam radius and height, respectively. Equation 3, derived by Elson and Madge, is based on the Stokes−Einstein relationship for Brownian diffusion,[64−66] and τ_D can be related to the diffusion coefficient, D, by

$$D = \frac{r^2}{4\tau_D} \tag{4}$$

dx.doi.org/10.1021/ac5039225 | Anal. Chem. 2015, 87, 83−98

Other fitting equations for additional types of diffusion have also been derived.[67,68] If various types of diffusion are present, a multiple component fit can be used to resolve heterogeneous behavior. Representative experimental results of $G(\tau)$ for different size probes ranging from 2 to 100 nm in size are shown in Figure 2C, demonstrating how FCS can reveal diffusion dynamic information based on the decay of the curve.

Advanced confocal microscopy and FCS techniques have been developed to circumvent limitations in traditional setups such as slow diffusion and signal from noncorrelated background. When transport is too slow, the diffusion coefficient cannot be accurately extracted due to long acquisition time required; the maximum lag time must be on the order of 5 000 times the longest characteristic diffusion time before the observed diffusion constant converges to the expected value.[69] Movement of the focal volume to parallelize the acquisition over the spatial dimension and reduce time points between data has been performed to analyze slower diffusion in techniques such as raster scan image correlation spectroscopy,[70−72] line scan FCS,[73,74] and circular scanning FCS.[75,76] Alternatively, multiple focal volumes separated by a set distance have been used in dual focus FCS to quantify the diffusion time from one focal volume to the other, obtaining information on a longer time scale in addition to the typical diffusion within each individual focal volume.[77−80] Methods such as two-photon excitation[81,82] or stimulated emission depletion (STED) geometry[83,84] improve analysis by reducing nonspecific excitation of the background and photobleaching for systems with high amounts of autofluorescence or optical aberrations causing noncorrealated background signal that obscures traditional autocorrelation analysis. Finally, alternatives for sample preparation have also allowed for nonfluorescent, unlabeled analyte to be observed by exploiting fluctuations in the fluorescent medium surrounding the particles in a technique called inverse FCS.[85−89] For further information on confocal microscopy techniques, specifically FCS, readers should refer to Elson,[63] Ries and Schwille,[90] and two reviews by Haustein and Schwille.[61,91]

Total Internal Reflectance Fluorescence Wide Field Imaging and Analysis. TIRF microscopy images single molecules over a wide field of view. TIRF limits the focal volume to be within ∼100 nm of the support/sample interface by using an exponentially decaying evanescent wave for excitation. The formation of the evanescent excitation wave is achieved by passing the excitation light at a high angle, θ, relative to the critical angle, θ_c, as defined by Snell's law, to allow for total internal reflection to occur at an interface:

$$\theta_c = \arcsin\left(\frac{\eta_2}{\eta_1}\right) \tag{5}$$

where η_1 and η_2 represent the refractive index of the substrate and sample, respectively. This high angle can be achieved through two possible geometries, either using a prism or passing the excitation at the edge of a high numerical aperture objective (Figure 2D). The totally internally reflected beam creates an evanescent wave that passes normal to the interface, and its penetration depth, d_p, decays exponentially according to

$$d_p = \lambda/4\pi\sqrt{\eta_1^2 \sin^2\theta - \eta_2^2} \tag{6}$$

where λ is the wavelength of the incident excitation. In typical TIRF measurements, $d_p \sim 100$ nm. The lateral size of the excitation in TIRF occurs over a wide field, typically ∼50 μm × 50 μm, allowing for a large area to be excited simultaneously. The resulting wide field of excitation can be detected on a 2D array detector, such as an electron multiplying charge coupled device (EMCCD), though newer scientific complementary metal-oxide semiconductor (CMOS) detectors are being used more often.[31] The resulting output, a movie comprised of a series of 2D images can be obtained at much faster time scales (∼10 Hz) than scanning confocal images and can resolve the dynamics of many molecules simultaneously. For further information on the instrumental details and applications on TIRF microscopy, readers should refer to Wazawa and Ueda[92] and Axelrod.[93]

Particle tracking analysis of TIRF data quantifies the diffusion dynamics of individual molecules. In particle tracking, molecules are identified in each frame, their locations are found and recorded, and the trajectories of the motion of the molecules from frame-to-frame are constructed by connecting molecule locations between frames. The single molecule trajectories can be further analyzed to understand the rate, nature, and distribution of diffusion (Brownian, anomalous, etc.) through mean square displacement analysis,[94−98] van Hove distributions,[99−101] radius of gyration,[102] and 3D spatial projections for curved interfaces.[103,104] Compared to FCS, the diffusion dynamics can be found for each individual molecule instead of requiring many individual events to calculate quantitative information. Further information on single molecule particle tracking methods can be found in reviews by Shuang et al.,[105] Saxton and Jacobson,[106] and Chenouard et al.[107]

Super-resolution imaging analysis of TIRF data can obtain spatial resolutions as small as ∼10 nm (Figure 2F). Since the general principles were introduced,[32,33,83,108,109] super-resolution methods have primarily been used to image biological structure but are finding increased application to synthetic materials and to understand dynamics. Fluorophores stochastically turn on and off through the image series either through photophysical control or adsorption/desorption[110] such that only a few fluorophores are "on" at a time within a single frame. This allows the centers of the isolated probes that appear as a diffraction limited spot (∼250 nm in size) to be localized with ∼10−20 nm precision by fitting to a 2D Gaussian or related point spread function model;[111,112] a statistical buildup of the locations of multiple "on" events leads to an image below the diffraction limit. Many reviews of super-resolution imaging have been reported recently and the impact and versatility of the technique was recognized by the Nobel Prize[113] in Chemistry in 2014.[40,114−116]

Progress in determining the orientation, three-dimensional location, and removal of photophysical events of single molecules has been realized in improvements to wide field TIRF microscopy. By defocusing the objective, the orientation of single molecules can be determined. First reported by Dickson et al.[117−120] with advances in analysis by Enderlein et al.,[121−123] defocusing changes the emission pattern of the fluorophores from an in-focus Airy disk to a defocused pattern indicative of the orientation of the emission dipole. Orientational imaging has addressed important questions in biological environments, such as molecular motors[124] and membranes,[125−129] and has advanced to incorporate super-resolution position[130] and chirality[131] information. Super-resolution imaging and tracking in the axial dimension, in addition to the lateral direction, has been achieved using phase masks[132−134] and multiplane collection geometries.[135−139] Phase masks introduce an optical astigmatism that, similar to defocusing, aberrates the emission pattern that indicates the z-location of single molecules. A simple

dx.doi.org/10.1021/ac5039225 | Anal. Chem. 2015, 87, 83−98

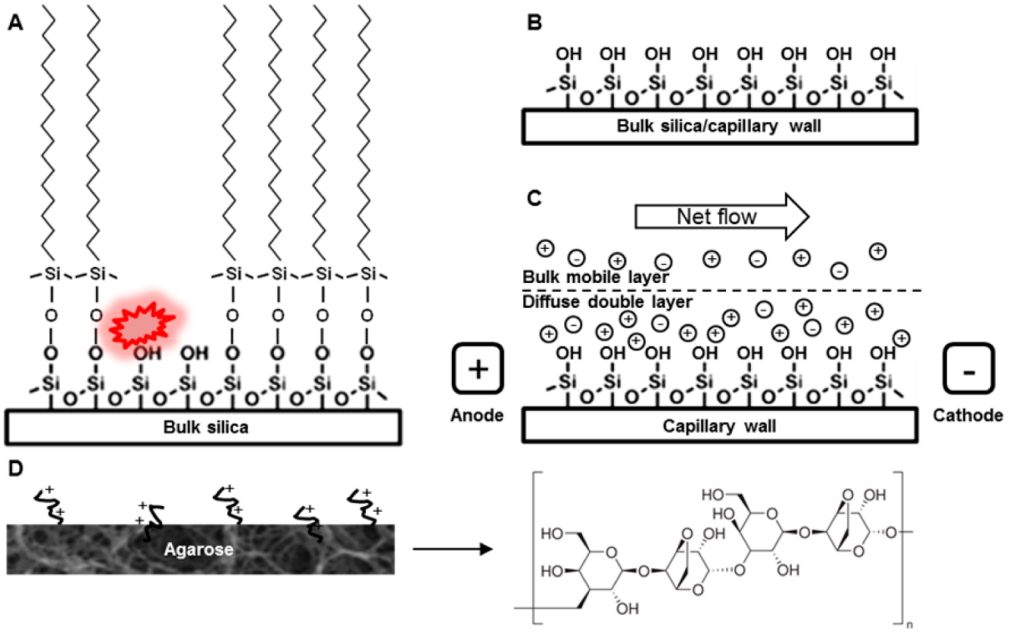

Figure 3. Illustration of different chromatographic interfaces studied by SMS. (A) C_{18} RPLC stationary phase with silanol defect present. In the articles reviewed, the single molecule fluorophore probes (represented by red burst) were observed to interact for long periods of time at defect sites but not at areas properly modified with octadecylorganosilane. (B, C) Silica-based stationary phases in (B) NPC/CLC and (C) CE where electro-osmosis of the surplus of cations in the double layer drives the mobile phase through the capillary to the cathode instead of hydrodynamic flow. (D) Anion-exchange IEX stationary phase with porous agarose support functionalized with clustered-charge cationic ligands. The chemical structure of agarose is included.

cylindrical lens placed in the detection path will lead to resolvable axial information to ~50 nm,[132,133] but the double-helix point spread function has been especially popular,[134,140,141] due to the ability to determine both 3D molecular orientation and position. Finally, alternating laser excitation (ALEX)[142,143] can perform "photophysical sorting" to discern dynamics from photophysics when two-color systems are being used. Two dye labels can be used to perform single molecule Förster resonance energy transfer (FRET), where the nonradiative transfer from one fluorophore ("donor") to the other ("acceptor") can be used to determine the distance between the dyes at 1−10 nm resolution.[144] Yet, blinking and bleaching of the donor and acceptor can lead to false artifacts and data assignments. In ALEX, two lasers are alternated, identifying and removing photophysical effects. When performed on a TIRF microscope with millisecond temporal resolution, dynamic information such as macromolecule-ligand adsorption can be resolved.[145]

Overall, SMS techniques reveal temporal and spatial information hidden in traditional ensemble techniques. Confocal and wide field TIRF microscopies resolve single molecules with a high signal-to-noise ratio using fluorescence to determine location, kinetic, diffusion, and orientation information. SMS has matured into a developed field with routine instrumentation and analysis that can be applied to understand chromatography at the fundamental concentration limit of a single molecule.

CHROMATOGRAPHY METHODS STUDIED BY SINGLE MOLECULE SPECTROSCOPY

Interfacial liquid chromatography systems, including reverse phase,[146−158] normal phase (silica based),[151,159−163] and ion-exchange[164−166] chromatography have been studied using SMS techniques (Figure 3). Chromatography can be classified based on the forces dominating the mobile/stationary phases interaction that in turn result in separation, e.g., hydrophobic/hydrophilic, electrostatic, steric, etc. In the following sections, each form of chromatography is introduced and the relevant SMS studies are reviewed.

Reverse Phase Liquid Chromatography. Reverse phase liquid chromatography (RPLC) utilizes a hydrophobic stationary phase to retain nonpolar analytes from a more hydrophilic mobile phase, usually consisting of a combination of water and acetonitrile. It is commonly applied to the separation of large hydrocarbon molecules not volatile enough to be separated by gas chromatography, making RPLC especially relevant to oil analysis. The preparation of the stationary phase is commonly performed through modification of silanol groups on a silica surface with an organosilane compound containing a hydrophobic moiety. The characteristics of the stationary phase are determined by the hydrophobic group, a long hydrocarbon such as C_{18} (Figure 3A). The ease of modifying silica microscopy coverslips with low amounts of autofluorescent contamination and the availability of nonpolar fluorescent molecules to use as probes has made RPLC very attractive for SMS studies.

The contribution of exposed RPLC stationary phase silanols to retention heterogeneity was studied using SMS. It has been known through ensemble studies that silanols can lead to complex energy distributions[167,168] within the stationary phase with an end result of tailing in the elution profile.[169,170] Wirth et al. was one of the first groups to apply single-molecule spectroscopy to RPLC to investigate surface heterogeneity.[146] On the basis of their early ensemble findings on the highly acidic and strong hydrogen-bonding properties of silanols that lead to tailing,[171] single molecule imaging and FCS were applied to the dynamics of the lipophilic cationic fluorescent probe, DiI, at a C_{18}-modified silica interface. In their first report,[146] two populations of diffusion were observed; a majority (99%) underwent fast diffusion ($D = 1.3 \times 10^{-6}$ cm^2/s) (Figure 4A), while a small population exhibited longer adsorptions with dwell times as long as 3.3 s (Figure 4B). These rare but long-lasting interactions were concluded to be the cause of tailing commonly

dx.doi.org/10.1021/ac5039225 | Anal. Chem. 2015, 87, 83−98

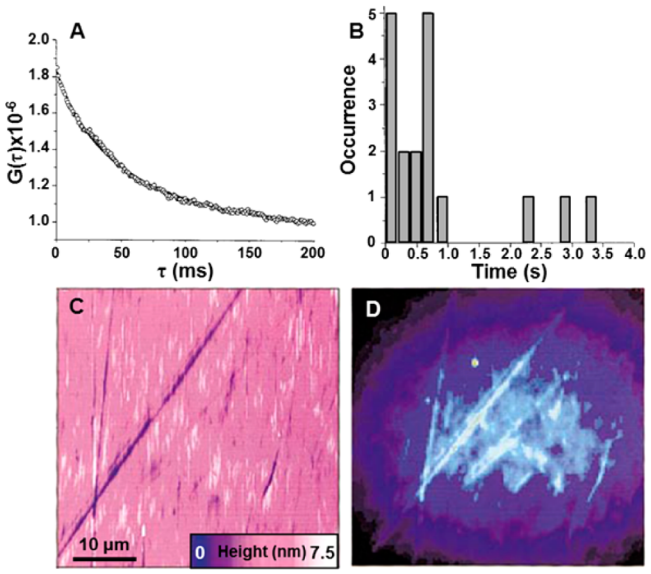

Figure 4. Identification of defect silanol sites leading to long-lived adsorption. (A) Fast diffusion was observed at nondefect sites through the FCS autocorrelation decay curve, while (B) strong, long-lasting adsorption was observed at suspected defect sites.[146] Correlated (C) AFM and (D) DiI fluorescent imaging at the C_{18} surface, showing strong adsorption takes place at defects.[147] Adapted and reprinted from refs 146 and 147. Copyright 1998 and 1999, respectively, American Chemical Society.

observed in RPLC. Further work correlated atomic force microscopy (Figure 4C) with fluorescent imaging (Figure 4D).[147] Longer adsorption sites were located at defects in the C_{18}-modified silica, implying exposed silanol groups were the source of the long events (Figure 3A).

The ability to tune the activity of these strong adsorption sites was studied through changing mobile phase conditions of acetonitrile[148] or methanol[149] content and pH.[147] Ludes and Wirth[148] varied the common RPLC variable of acetonitrile percentage while observing adsorption to the C_{18} interface. At increased acetonitrile concentration, the relative population of strong interactions of the analyte with characteristic desorption times of 0.07 s and 2.6 s, as quantified by confocal blip analysis, increased from 11% and 4% in water to 11% and 17%, respectively, in 60% acetonitrile. The 4-fold increase in the population of the longer 2.6 s desorption time is significant, as it contributes more to kinetic tailing under elution conditions. Mechanistic investigations through wide field fluorescent imaging confirmed adsorption was occurring at spatially distinguishable specific sites where polishing pits were present. By introducing propanol, it was found that the acetonitrile promotes adsorption by reducing the wetting of the specific adsorption sites.

In other early work, Harris et al. extracted adsorption kinetics in RPLC of cations with variable mobile phase methanol content.[149] Equations to analyze adsorption and desorption rate constants from FCS data collected in a total internal reflection excitation geometry were derived. Observing the adsorption of a cationic dye, rhodamine 6 G, to acidic silanols under increasing methanol concentrations up to 40%, it was found that the desorption rate decreases while the adsorption rate increases. One important conclusion from this work is that changes in the adsorption equilibrium constant with methanol cannot be explained by desorption rates only, and thus changes in the energy barrier to adsorption must be considered.

The RPLC separation of more complex analytes in the form of nucleic acids[150,151] using SMS showed heterogeneity due to interactions with exposed silanols that could be varied with pH. Oligonucleotides are known to hydrogen-bond, making RPLC the preferred purification technique. In Wirth and Swinton,[150] the transport of a fluorescently labeled 24-mer over C_{18} functionalized silica was investigated by confocal microscopy. FCS analysis showed bimodal diffusion where the diffusion coefficients differed by 2 orders of magnitude ($D_1 = 2 \times 10^{-8}$ and $D_2 = 2 \times 10^{-6}$ cm^2/s); the two populations were attributed to free diffusion and a distorted slow diffusion value due to adsorption events. Further investigation through blip analysis showed rare strong adsorption events up to 800 ms long. Again, strong adsorption was hypothesized to be due to hydrogen bonding of either the phosphate backbone or one or more of the oligomer bases to exposed surface silanols, leading to the peak tailing observed in bulk chromatography. In addition, fluctuations of the fluorescent signal of adsorbed oligonucleotides that could not be attributed to shot noise were observed, suggesting more rotational or partially adsorbed conformations were possible that were not observed in studies of DiI. Yeung et al. examined the adsorption of lambda-DNA to C_{18} surfaces and compared the results directly to commercial RPLC capillaries;[151] the single molecule observations of the total number of molecules adsorbed to the C_{18} interface and fraction of adsorbed molecules correlated with ensemble peak shapes under different pH conditions.

More recently, SMS studies of RPLC expanded to commercial materials[152,153] and used more complex analysis techniques.[154,155] Geng et al. were the first to look at a commercial support particle and observed rhodamine 6 G diffusion within C_{18} modified silica beads through FCS.[152] The diffusion properties were correlated to the spatial location within the bead (Figure 5A), showing the spatial heterogeneity of diffusion and adsorption dynamics, corresponding to the random distribution of silanol groups, consistent with the Wirth group findings.[146−148,150] Harris et al. used single particle tracking of the hydrophobic probe octadecylrhodamine B in C_{18} particles.[153] Single particle tracking offers diffusion information from a single molecule, compared to the many events required in FCS. The resulting trajectories (Figure 5B) showed that transport is not homogeneous; both diffusing and stuck molecules were observed and distinguished statistically. The analysis of diffusing molecules quantified the intraparticle diffusion coefficient to be $D = 3.1 \pm 0.1 \times 10^{-9}$ cm^2/s. For stuck molecules, the desorption times were correlated with the spatial location (Figure 5C). Importantly, it was found that there were statistically anomalous sites within the particle (Figure 5C, arrow) that exhibited both an increase in number of adsorption events and longer-lived desorption times, suggesting a positive correlation for a molecule to visit a site and fall into an energetically deep trap. Harris et al. also used FCS on images acquired on an EMCCD detector at rapid frame rates, combining the benefits of both spatial information on μm^2 scales from TIRF and temporal rates on millisecond time scales from FCS to study the heterogeneous diffusion rates of a hydrophobic probe at C_{18} and C_1 interfaces[155] and commercial particles.[156] Finally, Schwartz et al. have localized adsorption of BODIPY C_{12} fatty acids to anomalous defects at the trimethylsilyl stationary phase interface at ~50 nm resolutions using super-resolution imaging (Figure 5D) and were able to quantify an average coverage of 10−20 adsorption sites per square micrometer which

dx.doi.org/10.1021/ac5039225 | Anal. Chem. 2015, 87, 83−98

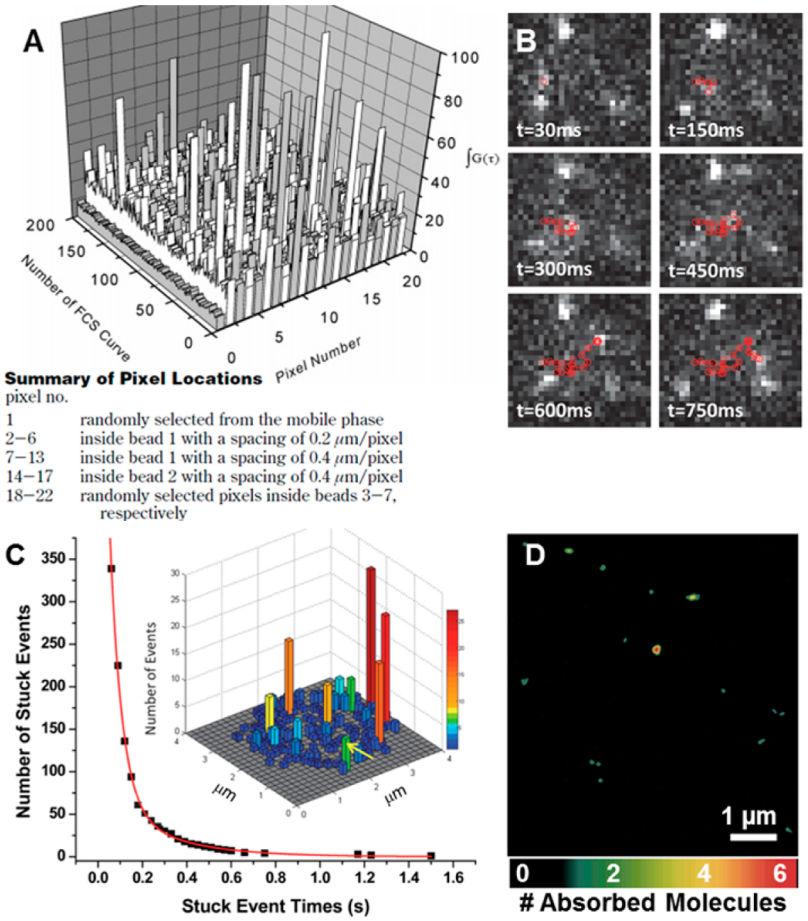

Figure 5. SMS performed in commercial RPLC particles. (A) Distribution of values for integrated autocorrelation curve of rhodamine 6 G diffusion at different locations within a commercial C_{18} stationary phase particle. A total of 200 trials per location were collected. The heterogeneity within the bead and over time are illustrated by the large spikes, indicating strong adsorption to an exposed silanol group.[152] (B,C) Spatially correlated tracking of diffusing and stuck single octadecylrhodamine B molecules in a commercial RPLC C_{18} particle. (B) Example trajectory (red dots/line) of diffusing molecule obtained by single molecule tracking shown at different frame times obtained through the measurement. (C) Histogram of octadecylrhodamine B adsorption dwell times for stuck molecules and (inset) the mapped spatial distribution of the total number of stuck events within the particle. An anomalously strong adsorption site indicated by a yellow arrow.[153] (D) Super-resolution map of single BODIPY C_{12} fatty acid adsorption to randomly dispersed defects at the trimethylsilyl interface.[154] Adapted and reprinted from refs 152, 153, and 154. Copyright 2005, 2013, and 2014, respectively, American Chemical Society.

would be otherwise unachievable by diffraction limited imaging.[154]

Overall, RPLC has been the most thoroughly studied chromatographic system using SMS due to the ease of preparing stationary phase with high purity required for SMS techniques and the importance of RPLC. SMS has been able to provide the universal observation that defect sites of available silanols leads to rare, long-lived adsorption for various analytes (DiI, rhoadamine 6G, nucleic acids, octadecylrhodamine B, C_{12} fatty acid) that can be spatially and temporally distinguishable from dominant faster, free diffusion and that prevention and tuning of these sites is critical to column performance in RPLC. The results have inspired further work modifying stationary phases by synthetic means[172,174] and simulations[173] to reduce and understand silanol prevalence. For further description of this foundational work, including kinetic results, see perspectives in Wirth, Swinton, and Ludes[157] and Wirth and Legg.[158]

Future work in RPLC could elucidate the role of the chemistry of the hydrophobic moiety (other than C_{18}) by using alternative groups, such as phenyls. Alternatives to silica, such as polymeric matrixes, that can perform RPLC at a wider range of pH values (silica is limited to pH 2–8) would also be of interest. Work on commercial particles in the spirit of Geng[152] and Harris[153,156] are especially promising to compare the performance of different suppliers at a molecular level. For example, if one particle performs better than another, is it due to the distribution of diffusion/displacement steps within pores or due to the number of exposed, active silanols? Advances in RPLC through SMS findings see much potential in the future.

Silica Surfaces: Normal Phase Chromatography and Capillary Methods. Silica interfaces play an important role in chromatography in separating polar organic and biomolecules. The acidic silica groups (Figure 3B) are used to retain polar molecules through hydrogen bonding from a less polar mobile phase, such as water-free *n*-hexane, chloroform, or ethyl acetate.[175] Silica interfaces are used in many forms of separations, most notably normal phase chromatography (NPC), capillary liquid chromatography (CLC), and the electrophoretic counterpart to the later, capillary electrophoresis (CE).

NPC, also called adsorptive chromatography, was one of the first forms of chromatography and was used most often in the first several decades of the technology, leading to the terminology "normal" (Figure 3B). In its most common form, the stationary phase is silica particles due to their desirable properties such as

dx.doi.org/10.1021/ac5039225 | *Anal. Chem.* 2015, 87, 83–98

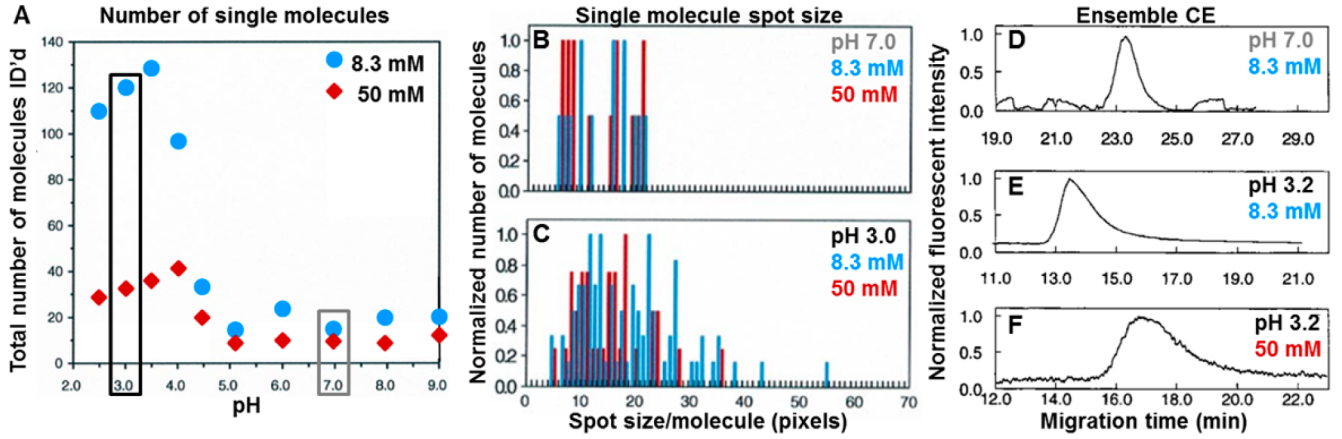

Figure 6. Single molecule and ensemble CE of protein adsorption to silica surface under different pH and ionic strength conditions. (A) Number of single molecules identified under varied pH at 8.3 and 50 mM buffer concentrations. pH values of 3.0 and 7.0 boxed for emphasis due to further study in parts B–F. (B, C) Spot size of single molecules observed at (B) pH 7.0 and (C) pH 3.0 and (blue) 8.3 and (red) 50 mM buffer concentration. The spot size is indicative of the diffusion properties of the protein near the surface. (D–F) Electropherograms at (E) pH 7.0, 8.3 mM; (E) pH 3.2, 8.3 mM; and (F) pH 3.2, 50 mM. The shapes of the electropherograms compared to the corresponding spot sizes in parts B and C are similar. Adapted with permission from Xu, X.-H. N.; Yeung, E. S. *Science* **1998**, *281*, 1650–1653 (ref 159). Copyright 1998 Science/AAAS.

ease of manufacturing, uniform size, ability to increase and control the surface area by using porous (with varying pore sizes) vs nonporous fused silica, and reasonable cost.[175] The silica can be further modified with polar chemical groups such as amino-, cyano-, or -diol phases.[176] Alternative, less commonly used stationary phase materials include alumina and carbon.

The methods of CLC (Figure 3B) and CE (Figure 3C) use the silica walls of a capillary for the stationary phase. The use of the capillary and/or electrophoretic force decrease the size and time-scale of separations. Though not a truly chromatographic process, CE is a very important technique used in the biotechnology and pharmaceutical industries to separate proteins, peptides, and nucleic acids. The electric field present in CE at the silica surface allows for electro-osmosis, moving the mobile phase toward the cathode based on the predominance of cations in the double layer (Figure 3C). Molecules are separated based on their electrophoretic mobility due to the interactions with the silica surface.

Silica surfaces can be easily modified for SMS as glass coverslips are abundantly used as substrates in microscopy. Silanization of the slides can easily be prepared through plasma cleaning or submersion in acidic, basic, or organic solutions based on the method employed.[177] Single molecule spectroscopists have been interested in silica surfaces from a foundational, interfacial science perspective,[178−182] yet only limited work has been performed on relating single molecule interfacial results to the application of chromatography.

Interfacial SMS studies of biomolecules at silica surfaces have been directly related to ensemble capillary techniques by Yeung et al. to demonstrate for the first time that SMS could predict experimental chromatographic elution peaks.[151,159−162] In their first studies, reported concurrently with the first SMS studies of RPLC, single protein adsorption to a fused silica surface was studied using wide field TIRF microscopy and the single molecule results were directly compared to ensemble CE results collected under similar conditions.[159] The pH and ionic strength were varied, and a mechanism for the observed single molecule results and ensemble CE peak broadening was presented based on the p*I* of the protein, silanol groups, and the electrical double layer. In the SMS results, as shown in Figure 6A, the number of adsorbed single concanavaline A proteins increased at decreased pH and decreased ionic strength. The results at pH 3.0 and 7.0 (boxed, Figure 6A) were further investigated. The size of the fluorescent spots recorded (Figure 6B,C), indicative of the diffusion of the protein near the interface, was also larger (hence, diffusion slower) at decreased pH and decreased ionic strength. The distribution of the fluorescent spot size corresponded well with the ensemble electropherograms (Figure 6D–F), where the peak symmetry decreased under decreased pH and ionic strength conditions. Correlating the results with the p*I* of the silanol groups and the protein and the predicted size of the electric double layer, it was concluded that long-range trapping of the protein beyond the electric double layer thickness occurs below the isoelectric point.

Yeung et al. further expanded their technique to understand other proteins[160] and DNA[151,161,162] (Figure 7A), revealing the importance of hydrophobic interactions between the analyte and stationary phase. In their initial studies of olglionucleuotides, λ-DNA with 12 unpaired bases at each end of the strand was studied under different pH and mobile phase solvent conditions.[151] The pH results offered important findings about the role of hydrophobicity in chromatography at polar silica interfaces. At decreased pH, hydrophobic properties of the unpaired bases dominated the separation over the traditionally viewed role of polarity and electrostatics. This was further studied by varying the number of unpaired bases where the λ-DNA was compared to PSP3 (19-unpaired bases) and double stranded DNA (0 unpaired bases).[161] As the number of bases increased, the ends became "stickier" under acidic conditions (Figure 7B), while no difference was observed under basic conditions (Figure 7C). This was explained based on the electrostatic, hydrophobic, and hydrogen-bonding properties of the analyte and silanols. Under basic conditions, both DNA and silanols are negative and the DNA is electrostatically repelled. However, below the silanol pK_a (~pH 6), the protonated silanols reduce the electrostatic repulsion of the DNA to the surface and the unpaired purine and pyrimidine bases adsorb the DNA to the surface through hydrophobic interactions. Similar to their results with concanavaline A, single molecule results of the distribution of adsorption times of the λ-DNA also correlated well with CLC chromatograms.[159]

dx.doi.org/10.1021/ac5039225 | *Anal. Chem.* 2015, 87, 83−98

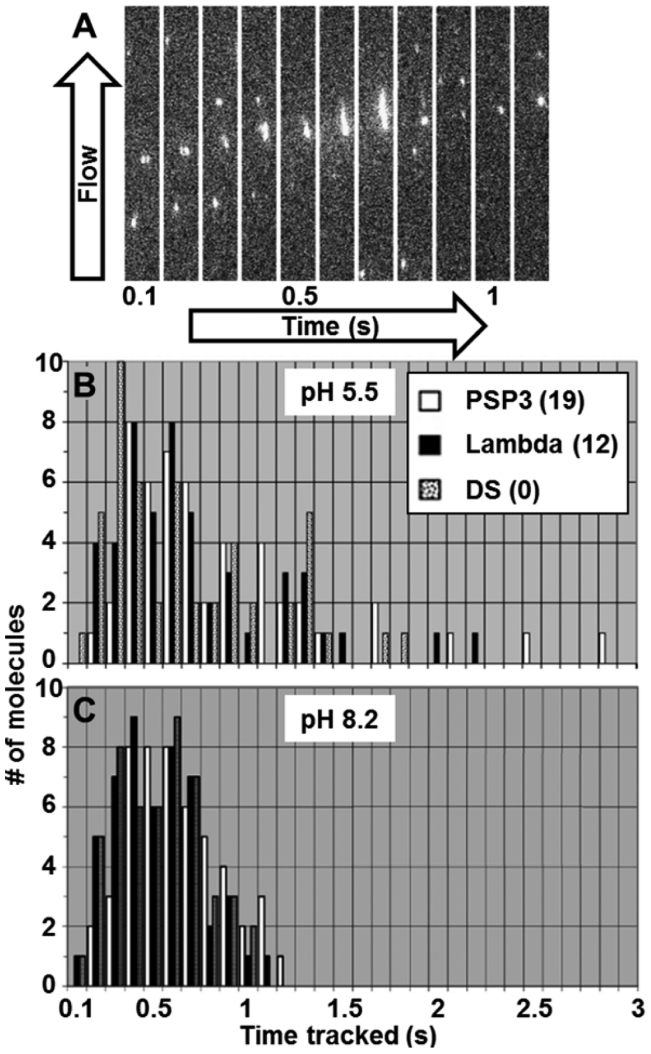

Figure 7. SMS studies of DNA at the water-silica interface. (A) Example single molecule image of immobilized and stretched DNA molecule (from 0.4 to 0.6 s). (B, C) Distribution of residence times of single DNA molecules with variable sticky end length (number of base pairs listed in legend after DNA name) under (B) acidic and (C) basic conditions. Adapted with permission from Isailovic, S.; Li, H.-W.; Yeung, E. S. *J. Chromatogr., A* **2007**, *1150*, 259−266 (ref 161). Copyright 2007 Elsevier.

Protein adsorption to silica was studied in Cuppet et al.[163] where TRITC-labeled lysozyme was observed under varying pH, ionic strength, and quality of silica polish to understand the importance of topography. Wide-field fluorescence and optical imaging and AFM were used to visualize adsorption and quantify the surface polishing defects. It was found that the lysozyme was reversibly bound at the heterogeneously distributed polishing marks. Reducing pH and increasing ionic strength caused the protein to desorb, suggesting short-range interactions, such as van der Waals, hydrogen bonding, acid−base, or conformation changes were the cause. Adsorption decreased when using superpolished silica, indicating topography was also a factor in adsorption and nonspecific adsorption could be prevented using these materials.[163]

The work on silica-based stationary phases shows that SMS can elucidate intermolecular interactions between the analyte and stationary phase and that single molecule results can be predictive of the expected ensemble behavior by comparing SMS results to CLC and CE collected under similar conditions. The results have addressed questions such as whether electrostatic or hydrophobic interactions are stronger and how external factors influence the behavior of biomolecules at the surface.[160] The findings have revealed that quality of the silica polishing and considerations on biomolecule structure are important.

SMS studies of polar-based stationary phases have thus far been limited to fused silica surfaces. There is much potential knowledge to be gained about modified silica with chemically grafted polar phases or porous silica where steric contributions will come into play. Sterics will also be significant in using multiple silica beads in packed NPC columns as opposed to the capillary methods studied by Yeung et al.,[151,159−162] so more advanced work correlating SMS results to NPC is needed. Potential studies of single molecules at the single or even multiparticle level, similar to what has been performed in RPLC,[152,153] could add insight. In regards to CE, SMS studies could be performed under applied potentials. The construction of electrochemical cells for single molecule[183] and single nanoparticle[184,185] systems have recently been reported in the literature and could be applied to understanding separations at silica interfaces driven by electro-osmosis.

Ion-Exchange Chromatography. Ion-exchange chromatography (IEX) separates molecules based on electrostatic affinity of the charged analyte to specific ionic functional groups in the stationary phase (Figure 3D). The stationary phase can be described as either anion-exchange (the anionic analyte exchanges with anions bound to positively charge ligands) or cation-exchange (the opposite). Common anion-exchange functional groups include triethylaminoethyl, polyethylenimine, *p*-aminobenzyl, or quaternary ammonium groups, and for cation-exchange, carboxymethyl, sufopropyl, phosphate, and sulfonate groups.[176,186] The functional ligands are typically supported on agarose (Figure 3D) or other cellulose derived matrixes due to their superior performance in protein separations, but silica or cross-linked polymers are also used in the high-pressure, high-performance liquid chromatography systems due to their low compressibility.[176] The porosity of the support matrix can be tuned to change the functional surface area available. Mobile phases are typically aqueous due to the ionization properties and solubility of salts and buffers in water. The ionic strength and pH of the mobile phase are critical to the exchange properties in IEX, since both affect the electrostatic distribution of charges on both the analyte and ligand.

IEX poses unique challenges to SMS sample preparation in comparison to silica modification in RPLC and NPC. Because agarose is biologically derived, autofluorescent impurities are difficult to eliminate. Selection of appropriate, high-purity materials must be performed to avoid false detection due to contamination or inability to resolve single molecules due to high background. Functionalization of the agarose support with the ligands also requires a more extensive chemical method of immobilization; for example, in Daniels et al.,[164] ion-exchange ligands were immobilized through first selectively activating aldehyde groups with periodate.[187] The amine-based ligands could then react with the activated aldehyde groups and are immobilized with the addition of cyanoborohydride. Finally, unreacted aldehyde sites are reduced with borohydride.

IEX at the single molecule level, studied by Landes et al., reveals the importance of the spatial distribution of ligand charge and the role of support matrix sterics.[164−166] Confocal microscopy and FCS were applied[164] in the tradition of Wirth et al.[157,158] as well as the first application of super-resolution

dx.doi.org/10.1021/ac5039225 | *Anal. Chem.* 2015, 87, 83−98

microscopy to chromatography,[166] to obtain subdiffraction spatial details. The spatial distribution of anion-exchange ligand charge in the stationary phase was compared between engineered, clustered-charge ligands in the form of penta-argininamide (Figure 8A) and traditional, single-charge ligands,

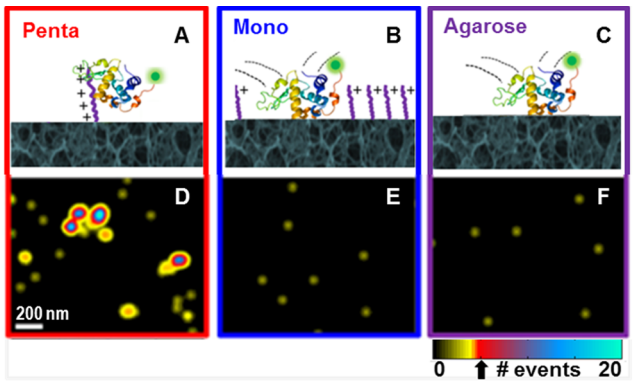

Figure 8. Super-resolution imaging demonstrates the importance of ligand charge distribution in ion-exchange chromatography. (A–C) Schemes and (D–F) super-resolution images of Alexa 555-labeled alpha-lactalbumin at (A, D) clustered-charge penta-argininamide functionalized agarose, (B, E) single-charged monoargininamide functionalized agarose, and (C, F) agarose control. Used with permission from Kisley, L.; Chen, J.; Mansur, A. P.; Shuang, B.; Kourentzi, K.; Poongavanam, M.-V.; Chen, W.-H.; Dhamane, S.; Willson, R. C.; Landes, C. F. *Proc. Natl. Acad. Sci. U.S.A.* **2014**, *111*, 2075–2080 (ref 166). Copyright 2014 National Academy of Sciences of the United States of America.

in the form of monoargininamide (Figure 8B). The unfunctionalized agarose support served as a control and fluorescently labeled alpha-lacatalbumin, a model globular protein, was used as a probe. Using the super-resolution imaging technique motion blur points accumulation for imaging nanoscale topography (mbPAINT),[110] Kisley et al. localized the specific interactions of the protein to the ligands. Only the engineered, clustered-charge penta-argininamide stationary phase induced detectable specific protein adsorption (Figure 8D), while the isolated, single-charge monoargininamide (Figure 8E) was indistinguishable from the agarose control (Figure 8F). The onset of specific clustered-charge capabilities of both the engineered, clustered-charged ligands and stochastic-clustered single-charged ligands at increased concentration was studied, showing that relying on stochastic clustering requires a 1 000-fold increase in charge density compared to engineered ligands with a charge-cluster greater than two. Further investigation into the kinetics demonstrated heterogeneity was reduced using the engineered clustered-charged ligands compared to stochastic-clustering of single charges that could possibly lead to a 5-fold increase in plate height.[166]

Super-resolution mbPAINT was then applied to the same system to obtain mechanistic insight into the relationship between increased ionic strength and a reduction in adsorption heterogeneity in IEX systems.[165] The kinetic results suggest that increased ionic strength both decreases the electrostatic interaction between the protein and ligand, as would be expected in an ion-exchange process, but also surprisingly revealed an additional steric contribution. Increased ionic strength decreases the swelling of the porous stationary phase support, leading to steric narrowing of ligand availability within the pores.[165]

The importance of the steric contribution of the agarose support in IEX was further supported by confocal microscopy studies in Daniels et al.[164] FCS and blip analysis were used to quantify the diffusion dynamics and affinity, respectively, of alpha-lactalbumin at glass, agarose, and penta-argininamide functionalized agarose interfaces. FCS showed a decrease in the diffusion coefficient of the protein near the surface of the agarose support compared to glass (Figure 9A,B) due to steric interactions. The presence of the ligand further slowed diffusion due to the additional electrostatic contribution (Figure 9C), and the spatial heterogeneity of ligand locations and steric availability with respect to the focal volume led to wide variability in diffusion dynamics (Figure 9C,D).

The work by Landes et al. has revealed the importance of the spatial distribution of charge for ligands and contributions of porosity and sterics in IEX. The onset of clustering and adsorption is consistent with previous ensemble studies at and above the studied threshold by Wu and Walters[188] and similar concepts on the importance of spatial distribution and onset concentration in bioadsorption of proteins and membranes to heterogeneous patchy polymer brushes have been observed.[189–191] The observed steric contribution is hypothesized to be one reason why affinity chromatography supports often utilize a "spacer arm" between the ligand and matrix.[192–194] The results by Landes et al. suggest that for real columns with multiple species in solution, not all proteins favor the same sites. Steric factors and the random charge-arrangement of an adsorption site would make different sites best suited for different proteins, as opposed to the most-favored sites for a given protein also being most-favored for all other proteins. Overall, the results help interpret a large body of previous results at the ensemble level by adsorption isotherms studying the heterogeneity and ligand structure in chromatography.[195–200]

Many future possibilities exist in SMS studies of IEX through advanced instrumentation and additional ligands and proteins. Unlike RPLC and NPC, IEX utilizes ligands on the stationary phase that could be fluorescently labeled in addition to the analyte. By expanding to a two-dye system, colocalization of both the stationary phase ligand and analyte could be performed. Applying single molecule FRET[201] and ALEX[142,143] techniques could elucidate distance and photophysical dynamics of the adsorbed analyte–ligand complex. Similarly, two-color studies could investigate the competition and variation in affinity between two different analytes for the same ligands. Application of SMS to different cation exchange ligands, IEX of nucleotides, and commercial particles are potential future avenues to study.

CONNECTING SINGLE MOLECULE DATA TO THE ENSEMBLE: THEORETICAL INSIGHT AND APPLICATION OF SINGLE MOLECULE SPECTROSCOPY DATA

Although SMS experiments offer insight on the molecular mechanisms occurring during chromatography, there is still the challenge of relating the data to actual chromatographic elution peaks and observables. Pasti et al.[202] have shown how to unify the stochastic theory of chromatography with single molecule and ensemble chromatography.[154,166,202,203] Experimental observables from SMS can now be used to inform, quantify, and predict the performance of chromatography via the theory. Likewise, SMS experiments can be used to improve and expand the theory itself.

dx.doi.org/10.1021/ac5039225 | *Anal. Chem.* 2015, 87, 83–98

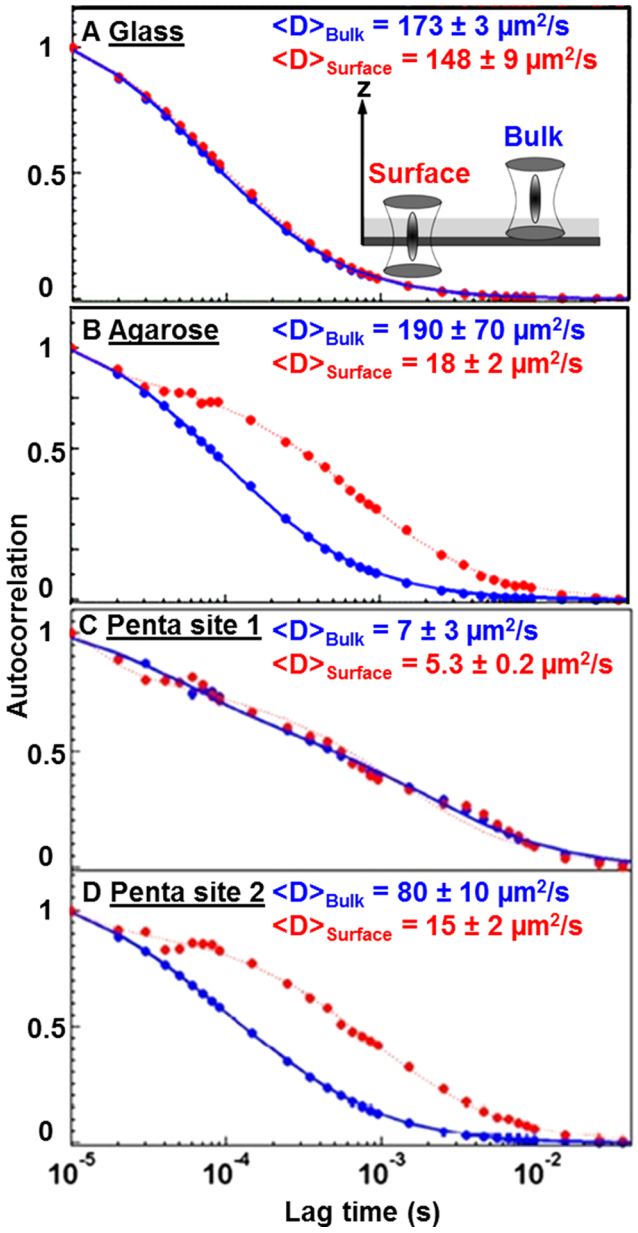

Figure 9. FCS results of protein dynamics at control and IEX interfaces with (A, inset) the focal volume located axially both in the bulk solution (blue) and near the surface (red). Diffusion over (A) glass substrate was identical to (B) bulk diffusion over agarose, but steric contributions are introduced near the surface. (C, D) Both electrostatics and sterics contribute to slowing diffusion of ligand-functionalized (in the form of clustered-charge cationic penta-argininamide) agarose and heterogeneity is observed at different locations of the sample due to spatial variation of peptides immobilized on the substrate. Adapted with permission from Daniels, C. R.; Kisley, L.; Kim, H.; Chen, W.-H.; Poongavanam, M.-V.; Reznik, C.; Kourentzi, K.; Willson, R. C.; Landes, C. F. *J. Mol. Recognit.* **2012**, *25*, 435−442 (ref 164). Copyright 2012 John Wiley and Sons, Inc.

While plate theory is the most common model used in separations science and provides a successful measure to compare column performance, it fails to relate the extracted theoretical variables of plate height (H) and number of plates (N) to any physical aspects of chromatography and is inexact in its use of the random walk model.[204] Also commonly used, the van Deemter equation[205] considers measurable quantities of molecular and Eddy diffusion and mass transfer kinetics. However, the equation is derived from a macroscopic perspective and is regularly either empirically or theoretically adjusted to account for individual conditions or more complex physical phenomena.[206,207] Alternatively, the stochastic theory of chromatography developed by Giddings and Eyring[208] is founded on a molecular basis and relates the dispersion of peaks in chromatography to molecular adsorption interactions. The theory is derived from a probabilistic approach of one solute molecule adsorbing to a single type of adsorption site based on the following equilibrium:

$$\mathrm{A} + \mathrm{I} \underset{k_d}{\overset{k_a}{\leftrightarrow}} [\mathrm{A{-}I}] \tag{7}$$

where A represents the analyte, I the interfacial stationary phase, and [A−I] the immobilized analyte interacting with the interface where the adsorption- and desorption-rates are described by k_a and k_d, respectively. Giddings and Eyring proposed that a Poisson distribution can represent the probability of a single analyte molecule associating with an adsorption site r_m times (r number of stochastic adsorption events for a given time, t, in the mobile phase, m):[208]

$$\psi_m = \frac{(k_a t_m)^{r_m}}{r_m!} \exp[-k_a t_m] \tag{8}$$

On the basis of eq 8, the stochastic theory has further been expanded for two-site and n-site adsorptions[209] but becomes increasingly complex as more sites are added, proving to be difficult to evaluate.

During the time when stochastic theory was being developed, the available ensemble experimental methods were an "n-site" problem,[209] making it impossible to relate ensemble experimental observables to theory. The advent of single molecule approaches revived the stochastic theory, as the conditions and observations are exactly what the theory is based on: single solute molecules adsorbing and desorbing at a single site. Experimental conditions also almost ideally meet the assumptions made in the theory where (1) adsorption−desorption kinetics dominate over diffusion (i.e., there is no Eddy diffusion) and (2) the adsorption/desorption rates are time-independent and independent of one another. Kisley et al. first confirmed the theory experimentally for a single-adsorption site, single-analyte system using super-resolution imaging.[166] Protein adsorption to individual anion-exchange ligands were observed and the kinetics were extracted from each ligand localized to ∼30 nm (Figure 10A). Each ligand exhibited single-exponential decay kinetics, validating that a nonvarying rate constant can describe each individual adsorption site and supports the stochastic model as a Poisson-distributed process. We are therefore at a point where SMS has made it possible to fill the gap noted by Giddings in his 1965 seminal work *Dynamics of Chromatography* that "empirical work has not yet offered the type of precise, discriminatory data needed [to synthesize a whole picture of chromatography down to the molecular world itself]".[204]

To relate single molecule data to the ensemble, Pasti et al. expanded the stochastic theory to use SMS results to model expected elution profiles.[202] The stochastic theory was modified to account for discontiuous distributions of adsorption times that are observed in SMS by incorporating the canonical Levy representation and relating it to the observed distribution of desorption times.[210] The Poisson distribution in eq 8 is first

dx.doi.org/10.1021/ac5039225 | *Anal. Chem.* 2015, 87, 83−98

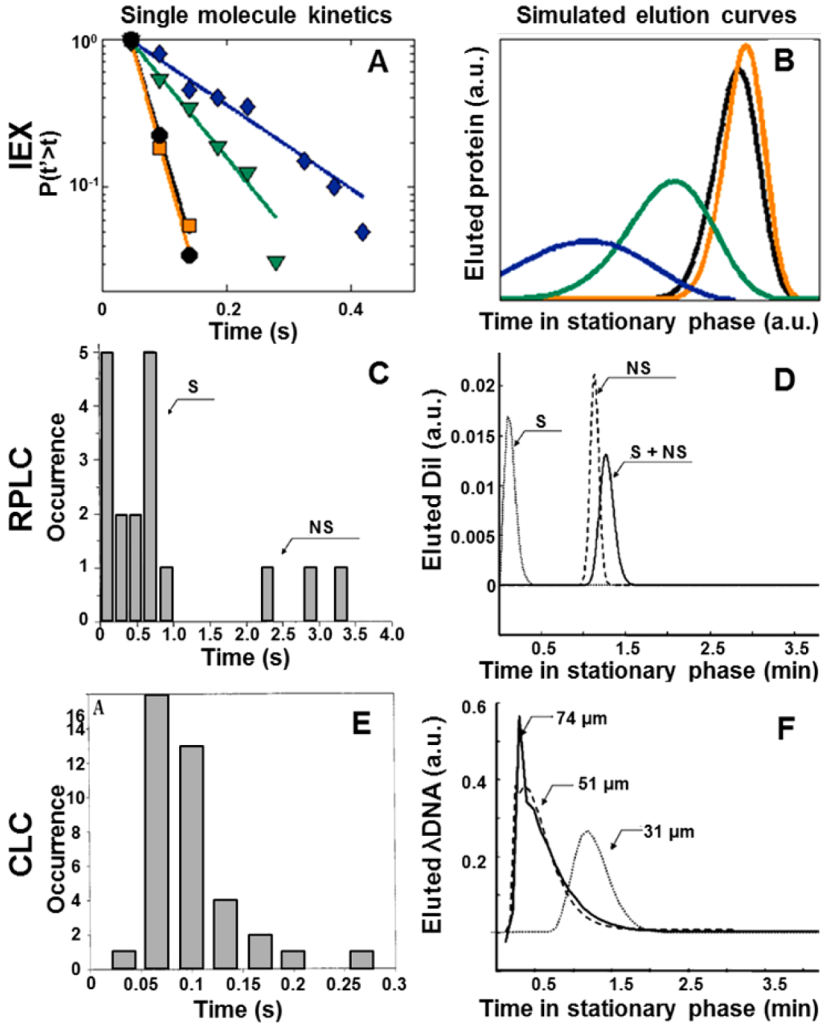

Figure 10. Applications of the stochastic theory of chromatography to use (A, C, E) single molecule kinetics to model (B, D, F) elution curves for (A, B) IEX, (C, D) RPLC, and (E, F) CLC. (A) Cumulative distribution of dissociation times of alpha-lactalbumin from individual penta-argininamide ligands shown with (B) respective modeled elution curves demonstrating interligand heterogeneity. (C) Histogram of dissociation times of DiI molecules at C_{18} with two populations of adsorption to specific (S) and nonspecific (NS) sites. (D) The resulting curves can separate the heterogeneous behaviors to show the contributions of the multicomponent behavior. (E) Histogram of dissociation times of λ-DNA molecules at the silica interface and (F) respective modeled curves with varying theoretical capillary diameter listed by varying r_m in eq 10. Images adapted from refs 146, 151, and 202 Copyright 1998, 2001, and 2005, respectively, American Chemical Society. Images adapted with permission from Kisley, L.; Chen, J.; Mansur, A. P.; Shuang, B.; Kourentzi, K.; Poongavanam, M.-V.; Chen, W.-H.; Dhamane, S.; Willson, R. C.; Landes, C. F. *Proc. Natl. Acad. Sci. U.S.A.* **2014**, *111*, 2075−2080 (ref 166). Copyright 2014 National Academy of Sciences of the United States of America.

converted to the frequency domain to express the stochastic process in the characteristic function formalism (ϕ) notation:[211]

$$\phi(t_s;\, \omega|t_m) = \exp[\mu t_m(\exp\{i\omega\tau_s\} - 1)] \tag{9}$$

where t_s is the overall time the analyte spends in the stationary phase, τ_s is the desorption time of each individual analyte adsorption event, and μ is the frequency of events. The Lévy formalism is then applied to accommodate the discontinuous single molecule distribution of τ_s:[210]

$$\phi(t_s;\, \omega|t_m) = \exp[r_m \sum_{i=1}^{i=k} (\exp\{i\omega\tau_{s,i}\} - 1)\Delta F(\tau_{s,i})] \tag{10}$$

where k is the index of the discrete set of desorption times given by $\Delta F(\tau_{s,i})$ that are observed in the single molecule experimental desorption time distributions. An inverse Fourier transform of eq 10 to the time domain is then used to extract $f(t_s)$, the simulated chromatographic peak:

$$\phi(t_s;\, \omega|t_m) \xrightarrow{F^{-1}} f(t_s) \tag{11}$$

Therefore, the single molecule observations, $\Delta F(\tau_{s,i})$, are unified to chromatographic peak distribution, $f(t_s)$. The resulting chromatograms obtained from single molecule experiment and analysis through the Levy-modified stochastic theory of chromatography can be evaluated in terms of the standard deviation of the peak to relate to plate theory if so desired. For a more thorough history and derivation of the mathematics used in this modeling, readers should refer to the review by Felinger.[203]

Application of Pasti et al.'s unifying elution curve modeling to findings in IEX, RPLC, and CLC chromatographic systems has been performed. In IEX, the kinetic results from individual ligands, as discussed above, have been used to model the expected elution curves given a single type of site (Figure 10B).[166] This further demonstrates the interligand heterogeneity that was caused by agarose sterics. Elution curve modeling has also been applied to IEX to demonstrate that engineered-

dx.doi.org/10.1021/ac5039225 | *Anal. Chem.* 2015, 87, 83−98

clustering of ligands[166] and increased ionic strength[165] can be used to reduce heterogeneity and improve efficiency. In RPLC, elution profile modeling demonstrated the impact of specific and nonspecific binding to silanol defect sites.[146,154,202] Two separate populations of retention were observed of DiI adsorbed to different areas of a C_{18} interface (Figure 10C), attributed to sites of different specific and nonspecific retention capabilities.[146] When modeling the expected elution curves (Figure 10D),[202] the two components were separated to reveal the contribution to the resulting combined profile. Nonspecific, long-lived interactions, though less frequently occurring, were shown to dominant the retention of the molecules, extending the elution time by approximately a factor of 4. Similar results were observed for BODIPY C_{12} fatty acid molecules at a trimethylsilyl interface.[154] The fraction and time spent by molecules at nonspecific and specific sites lead to simulated peak asymmetry from SMS results that were comparable to experimental chromatograms. Finally, modeling CLC separation of λ-DNA molecules at a silica interface showed the importance of capillary inner diameter in reducing the presence of tailing and elution time.[151,202] From the single molecule desorption time data (Figure 10E), the capillary diameter was varied in elution curve modeling by changing r_m in eq 10. As the capillary diameter was increased, the sorption rate from the mobile phase to the surface decreased, but tailing was more significant (Figure 10F). A comparison between the results shown in Figure 10 and the proposed capabilities in Figure 1 demonstrate the utility of SMS in resolving mechanistic heterogeneity and its contribution to the final peak shape and position through the stochastic theory of chromatography.

CONCLUSIONS AND FUTURE DIRECTION

SMS represents a unique method to understand chromatography from a molecular, mechanistic perspective. SMS techniques utilizing confocal and wide field TIRF microscopies have been developed and applied to RPLC, silica-based stationary phases, and IEX interfacial liquid chromatography systems. Results obtained by SMS have shown the importance of preventing stationary phase defects to reduce tailing in RPLC, the role of hydrophobic interactions in CLC/CE, the significance of the spatial distribution of charge for ligands and contributions of porosity in IEX, and that SMS results can adequately predict and model ensemble elution results.

There remain many unexplored systems in chromatography that could be investigated by SMS. Hydrophilic interaction,[212,213] size exclusion,[214] solid phase extraction,[215] supercritical fluid,[216] metal ion affinity,[217] counter-current,[218] and high temperature liquid[219−221] forms of chromatography/separation have yet to be studied by SMS. Future directions in modern chromatography include miniaturization of column technology with nanoparticle[10,222] and monolithic[14] columns and the use of membrane interfaces for separations.[223] SMS is ideal to study these systems due to the nanoscale spatial information that can be obtained through super-resolution imaging and demonstration of SMS analysis of molecular dynamics within polymers[224−227] that have been implemented in ensemble membrane separations.[228−230]

In future work, advanced SMS microscopy setups for multiple focal volume or two photon FCS, FRET,[201] defocusing,[121−123,131] 3D position, and ALEX,[142,143] could be applied to elucidate distance, conformation, orientation, or photophysical dynamics. Two-color excitation setups could investigate competitive interaction between multiple analytes at the stationary phase interface.

Overall, collaborations between the separation and SMS communities should continue, as to increase the understanding of chromatography from a molecular standpoint. Those in the separations field can identify unanswered questions plaguing chromatographic methods that cannot be understood through standard ensemble techniques, while single molecule spectroscopists can offer unique, advanced instrumentation and analysis. Interesting partnerships between single molecule spectroscopists and industry could reduce the time and cost of empirically determining column conditions. Many questions remain unanswered for future work in SMS of chromatography.

AUTHOR INFORMATION

Corresponding Author

*E-mail: cflandes@rice.edu.

Author Contributions

The manuscript was written through contributions of all authors. All authors have given approval to the final version of the manuscript.

Notes

The authors declare no competing financial interest.

Biographies

Lydia Kisley received her B.S. degree in Chemistry from Wittenberg University (Springfield, OH) in 2010, graduating *summa cum laude* with departmental honors. While at Wittenberg, she participated in two NSF Research Experiences for Undergraduates under Professor George Chumanov at Clemson University and Professor Bart Van Zeghbroeck at the University of Colorado at Boulder. She joined Professor Christy F. Landes' research group at Rice University to pursue her Ph.D degree in chemistry in the fall of 2010. She is a fellow of the National Science Foundation Graduate Research Fellowship Program as of spring 2012. Her research interests include single molecule spectroscopy, biomolecule−interface interactions, and molecular separations and diagnostics.

Christy F. Landes received her B.S. in Chemistry from George Mason University in 1998. She studied physical chemistry under the direction of Professor Mostafa El-Sayed at the Georgia Institute of Technology, earning her Ph.D. in 2003. After a postdoctoral position at the lab of Professor Geraldine Richmond at the University of Oregon, she was a National Institutes of Health Ruth L. Kirtschtein Postdoctoral Fellow under the direction of Professor Paul Barbara at the University of Texas at Austin. She joined the University of Houston as an Assistant Professor in 2006, later moving to Rice University. As of 2014, she is an Associate Professor of Chemistry and Electrical and Computer Engineering.

ACKNOWLEDGMENTS

C.F.L. thanks the NSF (Grants CBET-1134417 and CHE-1151647), the Welch Foundation (Grant C-1787), and the NIH (Grant GM94246-01A1) for support of this work. L.K. thanks the NSF for Graduate Research Fellowship 0940902. We thank L. J. Tauzin, C. Daniels, C. P. Byers, the Landes group members, and the S. Link and R. C. Willson research groups for collaboration and discussion.

REFERENCES

(1) Shire, S. J. *Curr. Opin. Biotechnol.* **2009**, *20*, 708−714.
(2) Henry, M. C.; Yonker, C. R. *Anal. Chem.* **2006**, *78*, 3909−3916.
(3) Walsh, G. *Nat. Biotechnol.* **2010**, *28*, 917−924.
(4) Dimitri, C.; Oberholtzer, L. *Marketing US Organic Foods: Recent Trends From Farms to Consumers*; Economic Research Service, U.S. Dept. of Agriculture, 2009.

(5) Blomberg, J.; Schoenmakers, P. J.; Brinkman, U. A. T. *J. Chromatogr., A* **2002**, *972*, 137−173.
(6) Santos, F.; Galceran, M. *TrAC, Trends Anal. Chem.* **2002**, *21*, 672−685.
(7) Chester, T. L. *Anal. Chem.* **2012**, *85*, 579−589.
(8) Patel, K. D.; Jerkovich, A. D.; Link, J. C.; Jorgenson, J. W. *Anal. Chem.* **2004**, *76*, 5777−5786.
(9) Gritti, F.; Leonardis, I.; Abia, J.; Guiochon, G. *J. Chromatogr., A* **2010**, *1217*, 3819−3843.
(10) Wei, B.; Rogers, B. J.; Wirth, M. J. *J. Am. Chem. Soc.* **2012**, *134*, 10780−10782.
(11) Wu, Z.; Wei, B.; Zhang, X.; Wirth, M. J. *Anal. Chem.* **2014**, *86*, 1592−1598.
(12) Rogers, B. J.; Wirth, M. J. *ACS Nano* **2012**, *7*, 725−731.
(13) Yang, Y.; Geng, X. *J. Chromatogr., A* **2011**, *1218*, 8813−8825.
(14) Guiochon, G. *J. Chromatogr., A* **2007**, *1168*, 101−168.
(15) Desmet, G.; Eeltink, S. *Anal. Chem.* **2012**, *85*, 543−556.
(16) Parastar, H.; Tauler, R. *Anal. Chem.* **2013**, *86*, 286−297.
(17) Hlushkou, D.; Gritti, F.; Daneyko, A.; Guiochon, G.; Tallarek, U. *J. Phys. Chem. C* **2013**, *117*, 22974−22985.
(18) Tsai, C. W.; Chen, W. Y.; Ruaan, R. C. *Langmuir* **2012**, *28*, 13601−13608.
(19) Moerner, W. E.; Fromm, D. P. *Rev. Sci. Instrum.* **2003**, *74*, 3597−3619.
(20) Moerner, W.; Kador, L. *Phys. Rev. Lett.* **1989**, *62*, 2535−2538.
(21) Orrit, M.; Bernard, J. *Phys. Rev. Lett.* **1990**, *65*, 2716−2719.
(22) Betzig, E.; Chichester, R. J. *Science* **1993**, *262*, 1422−1425.
(23) Xie, X. S.; Dunn, R. C. *Science* **1994**, *265*, 361−364.
(24) Macklin, J.; Trautman, J.; Harris, T.; Brus, L. *Science* **1996**, *272*, 255−258.
(25) Xie, X. S.; Trautman, J. K. *Annu. Rev. Phys. Chem.* **1998**, *49*, 441−480.
(26) Brooks Shera, E.; Seitzinger, N. K.; Davis, L. M.; Keller, R. A.; Soper, S. A. *Chem. Phys. Lett.* **1990**, *174*, 553−557.
(27) Whitten, W. B.; Ramsey, J. M.; Arnold, S.; Bronk, B. V. *Anal. Chem.* **1991**, *63*, 1027−1031.
(28) Funatsu, T.; Harada, Y.; Tokunaga, M.; Saito, K.; Yanagida, T. *Nature* **1995**, *374*, 555−559.
(29) Vale, R. D.; Funatsu, T.; Pierce, D. W.; Romberg, L.; Harada, Y.; Yanagida, T. *Nature* **1996**, *380*, 451.
(30) Schmidt, T.; Schütz, G.; Baumgartner, W.; Gruber, H.; Schindler, H. *Proc. Natl. Acad. Sci. U.S.A.* **1996**, *93*, 2926−2929.
(31) Michalet, X.; Colyer, R. A.; Scalia, G.; Ingargiola, A.; Lin, R.; Millaud, J. E.; Weiss, S.; Siegmund, O. H. W.; Tremsin, A. S.; Vallerga, J. V.; Cheng, A.; Levi, M.; Aharoni, D.; Arisaka, K.; Villa, F.; Guerrieri, F.; Panzeri, F.; Rech, I.; Gulinatti, A.; Zappa, F.; Ghioni, M.; Cova, S. *Philos. Trans. R. Soc. B* **2013**, *368*, 20120035.
(32) Rust, M. J.; Bates, M.; Zhuang, X. *Nat. Meth.* **2006**, *3*, 793−796.
(33) Betzig, E.; Patterson, G. H.; Sougrat, R.; Lindwasser, O. W.; Olenych, S.; Bonifacino, J. S.; Davidson, M. W.; Lippincott-Schwartz, J.; Hess, H. F. *Science* **2006**, *313*, 1642−1645.
(34) Tamarat, P.; Maali, A.; Lounis, B.; Orrit, M. *J. Phys. Chem. A* **1999**, *104*, 1−16.
(35) Daniels, C. R.; Reznik, C.; Landes, C. F. *Langmuir* **2010**, *26*, 4807−4812.
(36) Dickson, R. M.; Cubitt, A. B.; Tsien, R. Y.; Moerner, W. *Nature* **1997**, *388*, 355−358.
(37) Wu, B.; Piatkevich, K. D.; Lionnet, T.; Singer, R. H.; Verkhusha, V. V. *Curr. Opin. Cell Biol.* **2011**, *23*, 310−317.
(38) Chen, I.; Ting, A. Y. *Curr. Opin. Biotechnol.* **2005**, *16*, 35−40.
(39) Weiss, S. *Science* **1999**, *283*, 1676−1683.
(40) Ha, T.; Tinnefeld, P. *Annu. Rev. Phys. Chem.* **2012**, *63*, 595−617.
(41) Vogelsang, J.; Kasper, R.; Steinhauer, C.; Person, B.; Heilemann, M.; Sauer, M.; Tinnefeld, P. *Angew. Chem., Int. Ed.* **2008**, *47*, 5465−5469.
(42) Aitken, C. E.; Marshall, R. A.; Puglisi, J. D. *Biophys. J.* **2008**, *94*, 1826−1835.
(43) Shi, X.; Lim, J.; Ha, T. *Anal. Chem.* **2010**, *82*, 6132−6138.
(44) Dave, R.; Terry, D. S.; Munro, J. B.; Blanchard, S. C. *Biophys. J.* **2009**, *96*, 2371−2381.
(45) Campos, L. A.; Liu, J.; Wang, X.; Ramanathan, R.; English, D. S.; Munoz, V. *Nat. Methods* **2011**, *8*, 143−146.
(46) Rasnik, I.; McKinney, S. A.; Ha, T. *Nat. Methods* **2006**, *3*, 891−893.
(47) Altman, R. B.; Terry, D. S.; Zhou, Z.; Zheng, Q.; Geggier, P.; Kolster, R. A.; Zhao, Y.; Javitch, J. A.; Warren, J. D.; Blanchard, S. C. *Nat. Methods* **2012**, *9*, 68−71.
(48) Altman, R. B.; Zheng, Q.; Zhou, Z.; Terry, D. S.; Warren, J. D.; Blanchard, S. C. *Nat. Methods* **2012**, *9*, 428−429.
(49) Cooper, D.; Uhm, H.; Tauzin, L. J.; Poddar, N.; Landes, C. F. *ChemBioChem* **2013**, *14*, 1075−1080.
(50) Lakowicz, J. R. *Principles of Fluorescence Spectroscopy*; Springer: New York, 2006.
(51) Schmidt, T.; Schuetz, G. J.; Baumgartner, W.; Gruber, H. J.; Schindler, H. *J. Phys. Chem.* **1995**, *99*, 17662−17668.
(52) Kisley, L.; Chang, W.-S.; Cooper, D.; Mansur, A. P.; Landes, C. F. *Methods Appl. Fluoresc.* **2013**, *1*, 037001.
(53) Pal, R.; Beeby, A. *Methods Appl. Fluoresc.* **2014**, *2*, 037001.
(54) Hsiang, J.-C.; Jablonski, A. E.; Dickson, R. M. *Acc. Chem. Res.* **2014**, *47*, 1545−1554.
(55) Jablonski, A. E.; Hsiang, J.-C.; Bagchi, P.; Hull, N.; Richards, C. I.; Fahrni, C. J.; Dickson, R. M. *J. Phys. Chem. Lett.* **2012**, *3*, 3585−3591.
(56) Richards, C. I.; Hsiang, J.-C.; Senapati, D.; Patel, S.; Yu, J.; Vosch, T.; Dickson, R. M. *J. Am. Chem. Soc.* **2009**, *131*, 4619−4621.
(57) Willets, K. A.; Ostroverkhova, O.; He, M.; Twieg, R. J.; Moerner, W. E. *J. Am. Chem. Soc.* **2003**, *125*, 1174−1175.
(58) Bouffard, J.; Kim, Y.; Swager, T. M.; Weissleder, R.; Hilderbrand, S. A. *Org. Lett.* **2007**, *10*, 37−40.
(59) Butler, R. N.; Fahy, A. M.; Fox, A.; Stephens, J. C.; McArdle, P.; Cunningham, D.; Ryder, A. G. *Tetrahedron Lett.* **2006**, *47*, 1721−1724.
(60) Paige, J. S.; Wu, K. Y.; Jaffrey, S. R. *Science* **2011**, *333*, 642−646.
(61) Haustein, E.; Schwille, P. *Annu. Rev. Biophys. Biomol. Struct.* **2007**, *36*, 151−169.
(62) Duncan, R.; Bergmann, A.; Cousin, M.; Apps, D.; Shipston, M. *J. Microsc.* **2004**, *215*, 1−12.
(63) Elson, Elliot L. *Biophys. J.* **2011**, *101*, 2855−2870.
(64) Elson, E. L.; Madge, D. *Biopolymers* **1974**, *13*, 1−27.
(65) Aragón, S. R.; Pecora, R. *J. Chem. Phys.* **1976**, *64*, 1791−1803.
(66) Rigler, R.; Mets, Ü.; Widengren, J.; Kask, P. *Eur. Biophys. J.* **1993**, *22*, 169−175.
(67) Schwille, P.; Korlach, J.; Webb, W. W. *Cytometry* **1999**, *36*, 176−182.
(68) Piskorz, T. K.; Ochab-Marcinek, A. *J. Phys. Chem. B* **2014**, *118*, 4906−4912.
(69) Tcherniak, A.; Reznik, C.; Link, S.; Landes, C. F. *Anal. Chem.* **2008**, *81*, 746−754.
(70) Digman, M. A.; Brown, C. M.; Sengupta, P.; Wiseman, P. W.; Horwitz, A. R.; Gratton, E. *Biophys. J.* **2005**, *89*, 1317−1327.
(71) Digman, M. A.; Gratton, E. *BioEssays* **2012**, *34*, 377−385.
(72) Rossow, M. J.; Sasaki, J. M.; Digman, M. A.; Gratton, E. *Nat. Protoc.* **2010**, *5*, 1761−1774.
(73) Ries, J.; Chiantia, S.; Schwille, P. *Biophys. J.* **2009**, *96*, 1999−2008.
(74) Daniels, C. R.; Tauzin, L. J.; Foster, E.; Advincula, R. C.; Landes, C. F. *J. Phys. Chem. B* **2012**, *117*, 4284−4290.
(75) Petrášek, Z.; Schwille, P. *Biophys. J.* **2008**, *94*, 1437−1448.
(76) Ruan, Q.; Cheng, M. A.; Levi, M.; Gratton, E.; Mantulin, W. W. *Biophys. J.* **2004**, *87*, 1260−1267.
(77) Dertinger, T.; Pacheco, V.; von der Hocht, I.; Hartmann, R.; Gregor, I.; Enderlein, J. *ChemPhysChem* **2007**, *8*, 433−443.
(78) Chiantia, S.; Ries, J.; Kahya, N.; Schwille, P. *ChemPhysChem* **2006**, *7*, 2409−2418.
(79) Didier, P.; Godet, J.; Mély, Y. *J. Fluoresc.* **2009**, *19*, 561−565.
(80) Brinkmeier, M.; Dörre, K.; Stephan, J.; Eigen, M. *Anal. Chem.* **1999**, *71*, 609−616.
(81) Berland, K. M.; So, P.; Gratton, E. *Biophys. J.* **1995**, *68*, 694−701.
(82) Schwille, P.; Haupts, U.; Maiti, S.; Webb, W. W. *Biophys. J.* **1999**, *77*, 2251−2265.

(83) Hell, S. W.; Wichmann, J. *Opt. Lett.* **1994**, *19*, 780−782.
(84) Eggeling, C.; Ringemann, C.; Medda, R.; Schwarzmann, G.; Sandhoff, K.; Polyakova, S.; Belov, V. N.; Hein, B.; von Middendorff, C.; Schönle, A. *Nature* **2009**, *457*, 1159−1162.
(85) Wennmalm, S.; Thyberg, P.; Xu, L.; Widengren, J. *Anal. Chem.* **2009**, *81*, 9209−9215.
(86) Wennmalm, S.; Widengren, J. *Anal. Chem.* **2010**, *82*, 5646−5651.
(87) Sandén, T.; Wyss, R.; Santschi, C.; Hassaïne, G. r.; Deluz, C. d.; Martin, O. J.; Wennmalm, S.; Vogel, H. *Nano Lett.* **2011**, *12*, 370−375.
(88) Pal, N.; Verma, S. D.; Singh, M. K.; Sen, S. *Anal. Chem.* **2011**, *83*, 7736−7744.
(89) Wennmalm, S.; Widengren, J. *Front. Biosci.* **2011**, *S3*, 385−392.
(90) Ries, J.; Schwille, P. *BioEssays* **2012**, *34*, 361−368.
(91) Haustein, E.; Schwille, P. *Curr. Opin. Struct. Biol.* **2004**, *14*, 531−540.
(92) Wazawa, T.; Ueda, M. In *Advances in Biochemical Engineering/Biotechnology*; Rietdorf, J., Ed.; Springer: Berlin/Heidelberg, Germany, 2005; Vol. *95*, pp 77−107.
(93) Axelrod, D. *Traffic* **2001**, *2*, 764−774.
(94) Michalet, X. *Phys. Rev. E* **2010**, *82*, 041914.
(95) Michalet, X.; Berglund, A. J. *Phys. Rev. E* **2012**, *85*, 061916.
(96) Berglund, A. J. *Phys. Rev. E* **2010**, *82*, 011917.
(97) Shuang, B.; Byers, C. P.; Kisley, L.; Wang, L.-Y.; Zhao, J.; Morimura, H.; Link, S.; Landes, C. F. *Langmuir* **2013**, *29*, 228−234.
(98) Haiden, C.; Wopelka, T.; Jech, M.; Keplinger, F.; Vellekoop, M. J. *Langmuir* **2014**, *30*, 9607−9615.
(99) Wang, B.; Anthony, S. M.; Bae, S. C.; Granick, S. *Proc. Natl. Acad. Sci. U.S.A.* **2009**, *106*, 15160−15164.
(100) Wang, B.; Kuo, J.; Bae, S. C.; Granick, S. *Nat. Mater.* **2012**, *11*, 481−485.
(101) Skaug, M. J.; Mabry, J.; Schwartz, D. K. *Phys. Rev. Lett.* **2013**, *110*, 256101.
(102) Elliott, L. C.; Barhoum, M.; Harris, J. M.; Bohn, P. W. *Phys. Chem. Chem. Phys.* **2011**, *13*, 4326−4334.
(103) Oswald, F.; L. M. Bank, E.; Bollen, Y. J. M.; Peterman, E. J. G. *Phys. Chem. Chem. Phys.* **2014**, *16*, 12625−12634.
(104) Haas, B. L.; Matson, J. S.; DiRita, V. J.; Biteen, J. S. *Molecules* **2014**, *19*, 12116−12149.
(105) Shuang, B.; Chen, J.; Kisley, L.; Landes, C. F. *Phys. Chem. Chem. Phys.* **2014**, *16*, 624−634.
(106) Saxton, M. J.; Jacobson, K. *Annu. Rev. Biophys. Biomol. Struct.* **1997**, *26*, 373−399.
(107) Chenouard, N.; Smal, I.; De Chaumont, F.; Maška, M.; Sbalzarini, I. F.; Gong, Y.; Cardinale, J.; Carthel, C.; Coraluppi, S.; Winter, M. *Nat. Methods* **2014**, *11*, 281−289.
(108) Hess, S. T.; Girirajan, T. P. K.; Mason, M. D. *Biophys. J.* **2006**, *91*, 4258−4272.
(109) Sharonov, A.; Hochstrasser, R. M. *Proc. Natl. Acad. Sci. U.S.A.* **2006**, *103*, 18911−18916.
(110) Chen, J.; Bremauntz, A.; Kisley, L.; Shuang, B.; Landes, C. F. *ACS Appl. Mater. Interfaces* **2013**, *5*, 9338−9343.
(111) Parthasarathy, R. *Nat. Methods* **2012**, *9*, 724−726.
(112) Small, A.; Stahlheber, S. *Nat. Methods* **2014**, *11*, 267−279.
(113) "The Nobel Prize in Chemistry 2014". *Nobelprize.org*. Nobel Media AB 2014. Web. 2 Dec 2014 http://www.nobelprize.org/nobel_prizes/chemistry/laureates/2014/.
(114) Oddone, A.; Vilanova, I. V.; Tam, J.; Lakadamyali, M. *Microsc. Res. Tech.* **2014**, *77*, 502−509.
(115) Lippincott-Schwartz, J.; Manley, S. *Nat. Methods* **2009**, *6*, 21−23.
(116) Patterson, G.; Davidson, M.; Manley, S.; Lippincott-Schwartz, J. *Annu. Rev. Phys. Chem.* **2010**, *61*, 345−367.
(117) Bartko, A. P.; Dickson, R. M. *J. Phys. Chem. B* **1999**, *103*, 11237−11241.
(118) Bartko, A. P.; Dickson, R. M. *J. Phys. Chem. B* **1999**, *103*, 3053−3056.
(119) Bartko, A. P.; Xu, K.; Dickson, R. M. *Phys. Rev. Lett.* **2002**, *89*, 026101.
(120) Dickson, R. M.; Norris, D. J.; Moerner, W. E. *Phys. Rev. Lett.* **1998**, *81*, 5322−5325.
(121) Böhmer, M.; Enderlein, J. *J. Opt. Soc. Am. B* **2003**, *20*, 554−559.
(122) Dedecker, P.; Muls, B.; Deres, A.; Uji-i, H.; Hotta, J.-i.; Sliwa, M.; Soumillion, J.-P.; Müllen, K.; Enderlein, J.; Hofkens, J. *Adv. Mater.* **2009**, *21*, 1079−1090.
(123) Patra, D.; Gregor, I.; Enderlein, J. *J. Phys. Chem. A* **2004**, *108*, 6836−6841.
(124) Toprak, E.; Enderlein, J.; Syed, S.; McKinney, S. A.; Petschek, R. G.; Ha, T.; Goldman, Y. E.; Selvin, P. R. *Proc. Natl. Acad. Sci. U.S.A.* **2006**, *103*, 6495−6499.
(125) Huckabay, H. A.; Dunn, R. C. *Langmuir* **2011**, *27*, 2658−2666.
(126) Livanec, P. W.; Huckabay, H. A.; Dunn, R. C. *J. Phys. Chem. B* **2009**, *113*, 10240−10248.
(127) Armendariz, K. P.; Huckabay, H. A.; Livanec, P. W.; Dunn, R. C. *Analyst* **2012**, *137*, 1402−1408.
(128) Marchuk, K.; Ha, J. W.; Fang, N. *Nano Lett.* **2013**, *13*, 1245−1250.
(129) Gu, Y.; Ha, J. W.; Augspurger, A. E.; Chen, K.; Zhu, S.; Fang, N. *Nanoscale* **2013**, *5*, 10753−10764.
(130) Aguet, F.; GeissbŘhler, S.; Mńrki, I.; Lasser, T.; Unser, M. *Opt. Express* **2009**, *17*, 6829−6848.
(131) Cyphersmith, A.; Maksov, A.; Hassey-Paradise, R.; McCarthy, K. D.; Barnes, M. D. *J. Phys. Chem. Lett.* **2011**, *2*, 661−665.
(132) Huang, B.; Wang, W.; Bates, M.; Zhuang, X. *Science* **2008**, *319*, 810−813.
(133) Jones, S. A.; Shim, S.-H.; He, J.; Zhuang, X. *Nat. Methods* **2011**, *8*, 499−505.
(134) Backlund, M. P.; Lew, M. D.; Backer, A. S.; Sahl, S. J.; Grover, G.; Agrawal, A.; Piestun, R.; Moerner, W. *Proc. Natl. Acad. Sci. U.S.A.* **2012**, *109*, 19087−19092.
(135) Prabhat, P.; Ram, S.; Ward, E. S.; Ober, R. J. *IEEE Trans. Nanobiosci.* **2004**, *3*, 237−242.
(136) Prabhat, P.; Ram, S.; Ward, E. S.; Ober, R. J. In *Proceedings of SPIE on Three-Dimensional and Multidimensional Microscopy: Image Acquisition and Processing XIII*; SPIE: Bellingham, WA, 2006; p 60900L.
(137) Ram, S.; Chao, J.; Prabhat, P.; Ward, E. S.; Ober, R. J. In *Proceedings of SPIE on Three-Dimensional and Multidimensional Microscopy: Image Acquisition and Processing XIV*; SPIE: Bellingham, WA, 2007; p 64430D.
(138) Ram, S.; Kim, D.; Ober, R. J.; Ward, E. S. *Biophys. J.* **2012**, *103*, 1594−1603.
(139) Ram, S.; Prabhat, P.; Chao, J.; Ward, E. S.; Ober, R. J. *Biophys. J.* **2008**, *95*, 6025−6043.
(140) Lew, M. D.; Backlund, M. P.; Moerner, W. *Nano Lett.* **2013**, *13*, 3967−3972.
(141) Thompson, M. A.; Lew, M. D.; Badieirostami, M.; Moerner, W. E. *Nano Lett.* **2009**, *10*, 211−218.
(142) Kapanidis, A. N.; Laurence, T. A.; Lee, N. K.; Margeat, E.; Kong, X.; Weiss, S. *Acc. Chem. Res.* **2005**, *38*, 523−533.
(143) Kapanidis, A. N.; Lee, N. K.; Laurence, T. A.; Doose, S.; Margeat, E.; Weiss, S. *Proc. Natl. Acad. Sci. U.S.A.* **2004**, *101*, 8936−8941.
(144) Selvin, P. R. *Nat. Struct. Biol.* **2000**, *7*, 730−734.
(145) Margeat, E.; Kapanidis, A. N.; Tinnefeld, P.; Wang, Y.; Mukhopadhyay, J.; Ebright, R. H.; Weiss, S. *Biophys. J.* **2006**, *90*, 1419−1431.
(146) Wirth, M. J.; Swinton, D. J. *Anal. Chem.* **1998**, *70*, 5264−5271.
(147) Wirth, M. J.; Ludes, M. D.; Swinton, D. J. *Anal. Chem.* **1999**, *71*, 3911−3917.
(148) Ludes, M. D.; Wirth, M. J. *Anal. Chem.* **2001**, *74*, 386−393.
(149) Hansen, R. L.; Harris, J. M. *Anal. Chem.* **1998**, *70*, 4247−4256.
(150) Wirth, M. J.; Swinton, D. J. *J. Phys. Chem. B* **2001**, *105*, 1472−1477.
(151) Kang, S. H.; Shortreed, M. R.; Yeung, E. S. *Anal. Chem.* **2001**, *73*, 1091−1099.
(152) Zhong, Z.; Lowry, M.; Wang, G.; Geng, L. *Anal. Chem.* **2005**, *77*, 2303−2310.
(153) Cooper, J. T.; Peterson, E. M.; Harris, J. M. *Anal. Chem.* **2013**, *85*, 9363−9370.
(154) Mabry, J. N.; Skaug, M. J.; Schwartz, D. K. *Anal. Chem.* **2014**, *86*, 9451−9458.

(155) Cooper, J. T.; Harris, J. M. *Anal. Chem.* **2014**, *86*, 7618−7626.
(156) Cooper, J.; Harris, J. M. *Anal. Chem.* **2014**, DOI: 10.1021/ac503250a.
(157) Wirth, M. J.; Swinton, D. J.; Ludes, M. D. *J. Phys. Chem. B* **2003**, *107*, 6258−6268.
(158) Wirth, M. J.; Legg, M. A. *Annu. Rev. Phys. Chem.* **2007**, *58*, 489−510.
(159) Xu, X.-H. N.; Yeung, E. S. *Science* **1998**, *281*, 1650−1653.
(160) Kang, S. H.; Yeung, E. S. *Anal. Chem.* **2002**, *74*, 6334−6339.
(161) Isailovic, S.; Li, H.-W.; Yeung, E. S. *J. Chromatogr., A* **2007**, *1150*, 259−266.
(162) He, Y.; Li, H.-W.; Yeung, E. S. *J. Phys. Chem. B* **2005**, *109*, 8820−8832.
(163) Cuppett, C. M.; Doneski, L. J.; Wirth, M. J. *Langmuir* **2000**, *16*, 7279−7284.
(164) Daniels, C. R.; Kisley, L.; Kim, H.; Chen, W.-H.; Poongavanam, M.-V.; Reznik, C.; Kourentzi, K.; Willson, R. C.; Landes, C. F. *J. Mol. Recognit.* **2012**, *25*, 435−442.
(165) Kisley, L.; Chen, J.; Mansur, A. P.; Dominguez-Medina, S.; Kulla, E.; Kang, M.; Shuang, B.; Kourentzi, K.; Poongavanam, M.-V.; Dhamane, S.; Willson, R. C.; Landes, C. F. *J. Chromatogr., A* **2014**, *1343*, 135−142.
(166) Kisley, L.; Chen, J.; Mansur, A. P.; Shuang, B.; Kourentzi, K.; Poongavanam, M.-V.; Chen, W.-H.; Dhamane, S.; Willson, R. C.; Landes, C. F. *Proc. Natl. Acad. Sci. U.S.A.* **2014**, *111*, 2075−2080.
(167) Bandosz, T. J. *J. Colloid Interface Sci.* **1997**, *193*, 127−131.
(168) Pyda, M.; Stanley, B. J.; Xie, M.; Guiochon, G. *Langmuir* **1994**, *10*, 1573−1579.
(169) Nawrocki, J. *J. Chromatogr., A* **1997**, *779*, 29−71.
(170) Nahum, A.; Horváth, C. *J. Chromatogr., A* **1981**, *203*, 53−63.
(171) Wirth, M. J.; Fairbank, R. P.; Fatunmbi, H. O. *Science* **1997**, *275*, 44−47.
(172) Newby, J. J.; Legg, M. A.; Rogers, B.; Wirth, M. J. *J. Chromatogr., A* **2011**, *1218*, 5131−5135.
(173) Smith, E. A.; Wirth, M. J. *J. Chromatogr., A* **2004**, *1060*, 127−134.
(174) Moitra, N.; Ichii, S.; Kamei, T.; Kanamori, K.; Zhu, Y.; Takeda, K.; Nakanishi, K.; Shimada, T. *J. Am. Chem. Soc.* **2014**, *136*, 11570−11573.
(175) Snyder, L. R.; Kirkland, J. J.; Dolan, J. W. *Introduction to Modern Liquid Chromatography*; John Wiley & Sons: Hoboken, NJ, 2011.
(176) Cazes, J., Ed. *Encyclopedia of Chromatography*; Marcel Dekker: New York, 2001.
(177) Cras, J. J.; Rowe-Taitt, C. A.; Nivens, D. A.; Ligler, F. S. *Biosens. Bioelectron.* **1999**, *14*, 683−688.
(178) Kwok, K. C.; Yeung, K. M.; Cheung, N. H. *Langmuir* **2007**, *23*, 1948−1952.
(179) Kian Zareh, S.; Desantis, M.; Kessler, J.; Li, J.-L.; Wang, Y. M. *Biophys. J.* **2011**, *102*, 1685−1691.
(180) Kastantin, M.; Walder, R.; Schwartz, D. K. *Langmuir* **2012**, *28*, 12443−12456.
(181) Walder, R.; Kastantin, M.; Schwartz, D. K. *Analyst* **2012**, *137*, 2987−2996.
(182) Langdon, B. B.; Kastantin, M.; Schwartz, D. K. *Biophys. J.* **2012**, *102*, 2625−2633.
(183) Peterson, E. M.; Harris, J. M. *Langmuir* **2013**, *29*, 8292−8301.
(184) Peterson, E. M.; Harris, J. M. *Langmuir* **2013**, *29*, 11941−11949.
(185) Byers, C. P.; Hoener, B. S.; Chang, W.-S.; Yorulmaz, M.; Link, S.; Landes, C. F. *J. Phys. Chem. B* **2014**, DOI: 10.1021/jp504454y.
(186) Harris, D. C. *Quantitative Chemical Analysis*; W. H. Freeman and Company: New York, 2007.
(187) Afanassiev, V.; Hanemann, V.; Wölfl, S. *Nucleic Acids Res.* **2000**, *28*, e66.
(188) Wu, D.; Walters, R. R. *J. Chromatogr., A* **1992**, *598*, 7−13.
(189) Gon, S.; Santore, M. M. *Langmuir* **2011**, *27*, 1487−1493.
(190) Gon, S.; Santore, M. M. *Langmuir* **2011**, *27*, 15083−15091.
(191) Gon, S.; Kumar, K.-N.; Nüsslein, K.; Santore, M. M. *Macromolecules* **2012**, *45*, 8373−8381.
(192) Cuatrecasas, P. *J. Biol. Chem.* **1970**, *245*, 3059−3065.
(193) Cuatrecasas, P.; Wilchek, M.; Anfinsen, C. B. *Proc. Natl. Acad. Sci. U.S.A.* **1968**, *61*, 636.
(194) Rasmussen, J. K.; Gleason, R. M.; Milbrath, D. S.; Rasmussen, R. L. *Ind. Eng. Chem. Res.* **2005**, *44*, 8554−8559.
(195) Asish Xavier, K.; Willson, R. C. *Biophys. J.* **1998**, *74*, 2036−2045.
(196) Fu, J. Y.; Balan, S.; Potty, A.; Nguyen, V.; Willson, R. C. *Anal. Chem.* **2007**, *79*, 9060−9065.
(197) Gill, D. S.; Roush, D. J.; Shick, K. A.; Willson, R. C. *J. Chromatogr., A* **1995**, *715*, 81−93.
(198) Gill, D. S.; Roush, D. J.; Willson, R. C. *J. Chromatogr., A* **1994**, *684*, 55−63.
(199) Gill, D. S.; Roush, D. J.; Willson, R. C. *J. Colloid Interface Sci.* **1994**, *1*, 1−7.
(200) Xavier, A. K.; Willson, R. C. *Biophys. J.* **1998**, *74*, 2036−2045.
(201) Roy, R.; Hohng, S.; Ha, T. *Nat. Methods* **2008**, *5*, 507−516.
(202) Pasti, L.; Cavazzini, A.; Felinger, A.; Martin, M.; Dondi, F. *Anal. Chem.* **2005**, *77*, 2524−2535.
(203) Felinger, A. *J. Chromatogr., A* **2008**, *1184*, 20−41.
(204) Giddings, J. C. *Dynamics of Chromatography*; Marcel Dekker, Inc.: New York, 1965; Vol. *1*.
(205) Van Deemter, J. J.; Zuiderweg, F.; Klinkenberg, A. v. *Chem. Eng. Sci.* **1956**, *5*, 271−289.
(206) Gritti, F.; Guiochon, G. *J. Chromatogr., A* **2013**, *1302*, 1−13.
(207) Usher, K. M.; Simmons, C. R.; Dorsey, J. G. *J. Chromatogr., A* **2008**, *1200*, 122−128.
(208) Giddings, J. C.; Eyring, H. *J. Phys. Chem.* **1955**, *59*, 416−421.
(209) McQuarrie, D. A. *J. Chem. Phys.* **1963**, *38*, 437−445.
(210) Dondi, F.; Cavazzini, A.; Pasti, L. *J. Chromatogr., A* **2006**, *1126*, 257−267.
(211) Dondi, F.; Remelli, M. *J. Phys. Chem.* **1986**, *90*, 1885−1891.
(212) Yoshida, T. *J. Biochem. Biophys. Methods* **2004**, *60*, 265−280.
(213) Jandera, P. *Anal. Chim. Acta* **2011**, *692*, 1−25.
(214) Barth, H. G.; Boyes, B. E.; Jackson, C. *Anal. Chem.* **1996**, *68*, 445−466.
(215) Poole, C. F. *TrAC, Trends Anal. Chem.* **2003**, *22*, 362−373.
(216) Taylor, L. T. *Anal. Chem.* **2010**, *82*, 4925−4935.
(217) Porath, J. *Protein Express. Purif.* **1992**, *3*, 263−281.
(218) Foucault, A.; Chevolot, L. *J. Chromatogr., A* **1998**, *808*, 3−22.
(219) Yan, B.; Zhao, J.; Brown, J. S.; Blackwell, J.; Carr, P. W. *Anal. Chem.* **2000**, *72*, 1253−1262.
(220) Thompson, J. D.; Carr, P. W. *Anal. Chem.* **2002**, *74*, 1017−1023.
(221) Greibrokk, T.; Andersen, T. *J. Chromatogr., A* **2003**, *1000*, 743−755.
(222) Zhang, Z.; Wang, Z.; Liao, Y.; Liu, H. *J. Sep. Sci.* **2006**, *29*, 1872−1878.
(223) Wixom, R. L. G, C. W. *Chromatography: A Science of Discovery*; Wiley: Hoboken, NJ, 2010.
(224) Reznik, C.; Landes, C. F. *Acc. Chem. Res.* **2012**, *45*, 1927−1935.
(225) Wöll, D.; Braeken, E.; Deres, A.; De Schryver, F. C.; Uji-i, H.; Hofkens, J. *Chem. Soc. Rev.* **2009**, *38*, 313−328.
(226) Wang, S.; Jing, B.; Zhu, Y. *J. Polym. Sci. Polym. Phys.* **2014**, *52*, 85−103.
(227) Cherdhirankorn, T.; Best, A.; Koynov, K.; Peneva, K.; Muellen, K.; Fytas, G. *J. Phys. Chem. B* **2009**, *113*, 3355−3359.
(228) Rmaile, H. H.; Schlenoff, J. B. *J. Am. Chem. Soc.* **2003**, *125*, 6602−6603.
(229) Hong, S. U.; Bruening, M. L. *J. Membr. Sci.* **2006**, *280*, 1−5.
(230) Ouyang, L.; Malaisamy, R.; Bruening, M. L. *J. Membr. Sci.* **2008**, *310*, 76−84.